OPTIMUM DESIGN OF STIFFENED COMPOSITE PLATES UNDER IMPACT LOADING

by

Farzad Seyyedrahmani

B.S., Mechanical Engineering, Tabriz University, 2013

Submitted to the Institute for Graduate Studies in
Science and Engineering in partial fulfillment of
the requirements for the degree of
Master of Science

Graduate Program in Mechanical Engineering

Boğaziçi University

2019

ACKNOWLEDGEMENTS

First of all, I would like to express my deep gratitude to dear Prof. Fazil Onder Sonmez. He always had time for me and when I needed advice and support, he never hesitated to help. He is not only an outstanding academician but also a great man, I am very grateful to have the chance to get to know him.

I would like to thank my mother for her love and permanent support, my sister for her encouragements and my father for believing in me in every stages of my life. Without having these people behind me, there was no chances for any successes.

At the end, I would like to thank my friends Hamed, Nima, Mehdi, Sara, Mahsa and all friends who always had my back. I also thank my best friend and officemate Sina for his kindly support and friendship.

ABSTRACT

OPTIMUM DESIGN OF STIFFENED COMPOSITE PLATES UNDER IMPACT LOADING

Thin composite plates do not have sufficient strength and stiffness under transverse loads and bending moments. One may increase thickness, but using stiffeners is a more effective way of improving their mechanical response. Stiffeners are sections joined to a plate to increase its stiffness against out-of-plane deformation. Composite parts are subjected not only to static loads but also impact loads. Their safe use under impact loading should be ensured during design process. Because composite materials are generally used in weight-critical applications, they should be optimally designed to achieve the most effective use of material. There are numerous studies on the optimization of stiffened laminates under static loads, but few researchers attempted to optimize stiffened laminates under impact loading. The objective of this study is to develop a methodology to find the optimum design of stiffened composite plates subjected to low-velocity impact loads. The objective function to be minimized is taken to be the weight. A hat-stiffened composite plate is considered. The design variables are the dimensions of the stiffener. Three different constraints are imposed: Maximum deflection limit, delamination failure, and intralaminar failure. Thickness and fiber orientations are kept constant; but optimum results are obtained for different thicknesses. An explicit finite element model is developed in LSDYNA to simulate the response of the plate under impact loading. A modified simulated annealing algorithm is used to find the globally optimal design. A code is developed in ANSYS Parametric Design Language to implement the search algorithm and carry out finite element analyses. At the end, the optimum stiffened plates are compared with unstiffened composite plates under impact loading and their performances are evaluated for different loading conditions including static transverse loading.

ÖZET

DARBE YÜKÜ ALTINDAKİ BERKİTİLMİŞ KOMPOZİT PLAKALARIN OPTİMUM TASARIMI

İnce kompozit plakalar, enine yükler ve eğme momentleri altında yeterli dayanıma ve direngenliğe sahip değildir. Kalınlık artırılabilir, ancak berkiticiler kullanmak mekanik tepkilerini iyileştirmede daha etkili bir yoludur. Berkiticiler, düzlem dışı deformasyona karşı direngenliği arttırmak için plakaya birleştirilen parçalardır. Kompozit parçaların darbe yükü altında güvenli kullanımları tasarım sürecinde sağlanmalıdır. Kompozit malzemeler umumiyetle ağırlığı önem taşıyan uygulamalarda kullanıldığından, malzemenin en etkin kullanımını sağlamak için optimum şekilde tasarlanmaları gerekir. Statik yükler altında berkitilmiş laminatların eniyilemesi üzerine çok sayıda araştırma yapılmıştır, ancak az sayıda araştırmacı darbeli yükleme altında berkitilmiş laminatları eniyilemeyi denemiştir. Bu çalışmanın amacı, düşük hızlı darbe yüklerine maruz berkitilmiş kompozit plakaların optimum tasarımını bulmak için bir yöntem geliştirmektir. Değerini en aza indirmek üzere gaye fonksiyonu olarak ağırlık alındı. Şapka şeklinde berkitilmiş bir kompozit plaka ele alındı. Berkiticinin boyutları tasarım değişkenleri olarak kabul edildi. Üç farklı sınırlama uygulandı: Azami sapma limiti, katman ayrışması ve katman içi kırılma. Kalınlık ve elyaf yönleri sabit tutuldu; ancak farklı kalınlıklar için optimum sonuçlar elde edildi. Plakanın darbe yükü altında tepkisinin benzeşim modelini oluşturmak için LSDYNA'da bir sonlu elemanlar modeli geliştirildi. Global optimum tasarımı bulmak için bir yenilenmiş tavlama simülasyonu algoritması kullanıldı. Arama algoritmasını uygulamak ve sonlu elemanlar analizi yapmak için ANSYS Parametrik Tasarım Dili'de bir kod geliştirildi. Son olarak, optimum berkitilmiş plakalar darbeli yükleme altındaki berkitilmemiş düz kompozit plakalarla karşılaştırıldı ve performansları statik enine yükleme dâhil olmak üzere farklı yükleme koşulları için değerlendirildi.

TABLE OF CONTENTS

LIST OF FIGURES

LIST OF TABLES

LIST OF SYMBOLS

A_b	Cross-sectional area
c_i	Weight coefficient
$[C]$	Damping matrix
F_{obj}	Objective function
$F(t)$	Load vector
g	gravitational acceleration
$[K]$	Stiffness matrix
$[M]$	Mass matrix
t_s	Thickness
u	Nodal displacement vector
W	Weight
W_0	Initial weight
δ_i	Initial distance
δ_f	Final distance
ρ	Density

LIST OF ACRONYMS/ABBREVIATIONS

2D	Two Dimensional
3D	Three Dimensional
APDL	ANSYS Parametric Design Language
CFRP	Carbon Fiber Reinforced Polymer
DOF	Degree of Freedom
FEA	Finite Element Analysis
FEM	Finite Element Modelling
FRP	Fiber Reinforced Plastic
GFRP	Glass Fiber Reinforced Polymer
MSA	Modified Simulated Annealing
SA	Simulated Annealing

1. INTRODUCTION

1.1. Background

Composite materials are one of the high demand materials in the industry, mostly, because of their high strength in spite of their light weight. Composites are usually made up of two constituents; their combination imparts superior characteristics to the material compared to separate properties. These constituents include fibers that are mostly made of glass or carbon, and a matrix which can be a polyester, epoxy, or another polymer resin. Fibers add rigidity and prevent crack propagation while matrix holds the fibers and provides compressional strength to the combination. Metals are equally strong in all directions however composites can be engineered to obtain different features such as high strength by choosing proper reinforcement and fiber direction in each ply. Major advantages of laminated composite panels are:

- High stiffness-to-weight ratio and strength-to-weight ratio
- Tailorability for specific design requirements
- High fatigue endurance limit
- High durability and damage tolerance
- High corrosion resistance

Composite materials are being used more and more in vehicles as replacement of metal parts to reduce weight in order to achieve fuel economy or longer ranges for electric vehicles. The body of a vehicle can be made of thin composite panels. With the use of stiffeners, sufficient rigidity can be achieved. As another concern in the design of vehicles, crashworthiness is an important requirement for the safety of passengers during collisions. Stiffeners can be attached to the inner faces of the door panels to increase crashworthiness of the vehicle in the event of high-speed collisions or decrease the likelihood of damage to the door panels during low-speed collisions.

Because composite materials have very high strength and stiffness-to-weight ratio, thin composite plates can satisfy in-plane strength and stiffness requirements; but they do not have sufficient strength and stiffness under transverse loads and bending moments. One may increase thickness to impart greater strength and stiffness; but this will significantly increase weight. Considering that composites are mostly used in weight-critical applications, choosing a larger thickness is not an acceptable option. On the other hand, using stiffeners is an effective way of improving the mechanical response without considerable increase in weight. Stiffeners are sections joined to a plate to increase its stiffness against out-of-plane deformation. Using stiffeners, one may significantly increase flexural strength as well as flexural stiffness of plates, thus improve buckling strength and transverse vibration properties. There are a variety of stiffener sections as can be seen in Figure 1.1 [1].

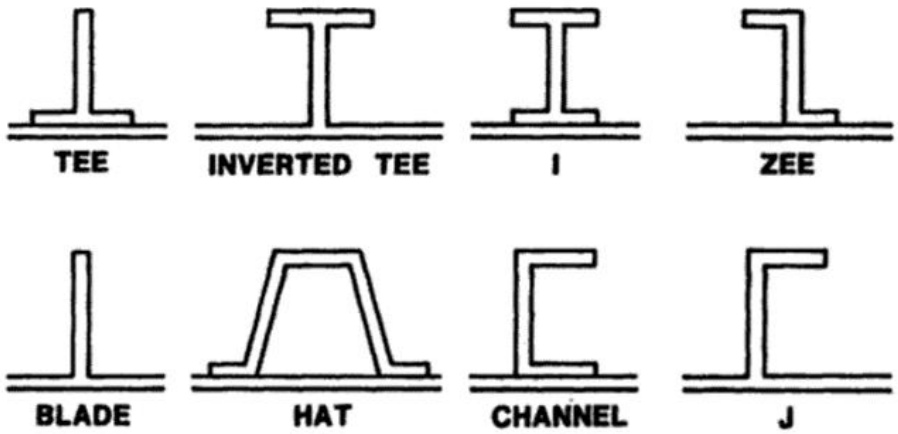

Figure 1.1. Types of stiffeners [1].

Composite parts are commonly subjected to impact loads; collision of two cars, birds striking airplanes, and dropping an object onto a composite structure are examples of impact loadings. Unlike metals, which are good energy absorbers due to their high ductility, composites are brittle and without losing their structural integrity, they can absorb energy mostly in the elastic region. There are two types of impact loading; high-velocity impact and low-velocity impact. One important difference between them is the contact time in the impact incident. In high-velocity impact, contact time is quite short, and the structure is usually not able to absorb adequate amount of impact

energy. So, the resulting damage is limited to the neighborhood of the impact area. In contrast, in low-velocity impact the impact time is long; if impact energy is not large, the whole structure can absorb the impact energy in the elastic region; however, if the energy is larger than the energy absorbing capacity of the composite structure, a catastrophic failure may occur. If impact loads are expected during the use of a structural part, it should be designed to have sufficient impact resistance.

Considering expensive cost of the composite materials and their use in weight-critical applications like aerospace, it is important to reduce use of raw materials by weight optimization. The aim of weight optimization is to determine the design with the lowest weight while it satisfies all the design goals.

1.2. Literature Review

1.2.1. Structural Behavior of Stiffened Plates

Numerous studies were conducted to investigate the structural response and failure behavior of stiffened composite structures under various loading conditions. Yap *et al.* [2] analyzed the influence of debonding between the stiffener and the skin in a T-stiffened laminated plate in the post-buckling range to evaluate critical parameters such as debond type, debond size, debond location, and plies lay-up. They used finite element (FE) modeling and fracture mechanics to anticipate the crack growth. Their results showed that local and global buckling were critical parameters in debonding initiation. Goswami [3] studied first-ply failure of stiffened/ unstiffened composite laminates under static loading using FE method and Tsai-Wu failure criterion. Prusty [4] investigated the progressive failure of transversely loaded stiffened composite panels using FE method and first-order shear deformation theory. The failure analysis of the stiffener and the plate was performed ply by ply and the critical load was obtained for various ply orientations. Xie and Chapman [5] presented a logical design method for transverse stiffeners. Their method was based on tension field theory in which external forces caused axial compression in a stiffened plate. By implementing the method, they could evaluate the axial force developed in the stiffener during non-linear elastic

buckling using FE analysis of. Gan *et al.* [6] experimentally and analytically studied energy absorption of a grid-stiffened laminate under transverse loading. They performed experimental tests and simulations using ABAQUS software in three-point bending. According to their results, grid-stiffened panels showed great damage tolerance. Moreover, when the loading is applied on the rib side, energy absorption is higher and deflection is less compared to the case in which the load is applied load on the skin side. Bedair [7] showed the behavior of stiffened thin-walled plates under static and dynamic loads. He investigated some major parameters in the design of stiffened plates such as the effects of stiffener dimensions on the strength and the numbers of stiffeners in the plate. Frulla *et al.* [8] applied compressive forces to damaged stiffened plates to assess the structural behavior of them. Under local buckling and global buckling, the strain distribution was obtained, and a preliminary fatigue test was performed. Lee *et al.* [9] tried to find the minimum stiffness needed for transverse stiffened concrete filled tube using column buckling approximation. They analytically evaluated several parameters on elastic and inelastic strength of the stiffened plate by considering the local buckling. They also modeled a stiffened panel under uniform compressive stress using finite element analysis. Found *et al.* [10] experimentally examined impact loading on blade shaped- stiffened CFRP plates and compared the preliminary results with unstiffened ones. In another experimental work on stiffened plates, low-velocity impact load was applied on the skin of stringer-stiffened laminated structures in order to evaluate damage shapes and damage distribution through the thickness [11].

1.2.2. Optimization of stiffened composites under various loads

Because of considerable benefits of stiffeners, there are many studies in the literature on the design optimization of stiffened composite structures. Upadhyay and Kalyanaraman [12] optimized a simply supported stiffened composite panel subjected to compression and in-plane shear loading. They considered stability and strength as constraints. They used a genetic algorithm to solve the problem. They considered type and number of stiffeners, dimensions, number of layers, fibers orientations, and lamina thickness as design variables. In another study, Stroud and Anderson [13] tried to

minimize the weight of a composite stiffened rectangular panel under combined loads. All geometric parameters were taken as variables including layer thickness and orientation angles. Constraints were imposed on buckling and material strengths, stiffness, and vibration frequency. In order to achieve optimization, they used feasible direction algorithm. Although the structural behavior depends on the number of plies and their angles, the optimization problem becomes more tractable, if the designer predetermines the thickness of the laminate and limits the variety of their angles [14]. In this case, the optimization problem is a stacking sequence problem as in study by Nagendra *et al.* [15]. They used genetic algorithm in order to find the optimum design of a stiffened composite panel. In another study, Negandra *et al.* [16] modified the genetic algorithm to decrease the cost of the process to design a stiffened panel with blade stiffeners under the axial and shear loads by minimizing its weight. One method to minimize the weight of T-stiffened and hat-stiffened laminated panels was presented by Bushnell and Bushnell [17]. PANDA 2 program was used to design a laminated composite to minimize the weight of the panels or shells. The applied loads were normal pressure, edge moments, and temperature in their model. They also considered transverse shear deformation effect. They considered the thickness of the plies, ply orientation angles, and all the dimensions as design variables. They assumed several constraints for the design such as local and general buckling, and the maximum stress. In one study, Wang *et al.* [18] investigated thermal residual stresses in a stiffened composite plate to improve the free vibration properties by maximizing the first natural frequency. For this purpose, they considered an unconstrained stiffened plate with no mechanical loads and tried to determine the optimal locations of the stiffeners. They predetermined the number of the stiffeners and obtained their optimum locations using the moving asymptotes method. Rikards *et al.* [19] used response surface methodology to build a surrogate model of laminated stiffened panels. They used a genetic algorithm to minimize the weight with buckling and post-buckling constraints. Upper and lower edges were fixed in clamping boxes and loading was axial compression. The variables were discrete thickness and number of stiffeners.

1.2.3. Studies on the effects of low-velocity impact loading on composites

Composite structures under impact loading can fail in several modes. For this reason, impact damage is a major concern in their design. In metals, impact damage is observed on the surface while in composites, damage can begin on the non-impacted surface [20]. As a result, inter-laminar stresses should be considered important as well as intra-laminar failure modes. There are numerous studies about impact loading considering damage modes, energy absorbing characteristics, and impact resistance. Impacts can be classified as low-velocity and high-velocity impacts. According to Sjoblom *et al.* [21] and Shivakumar *et al.* [22], low velocity impact is a quasi-state event and the upper limit on impact speed is between one to 10 m/s. Strait *et al.* [23] investigated the effects of stacking sequence on the impact resistance by penetration tests. They evaluated five layup geometries which were balanced and symmetric, cross-ply, quasi-isotropic layups and layups with 0, +45 and -45 degree plies. Aslan *et al.* [24] conducted impact tests to examine the effect of impact on glass-fiber reinforced cross-ply composites. They carried out finite element analyses to obtain stresses, contact forces, and failure analysis in order to predict delamination initiation. In the failure analysis, they considered two criteria: A criterion for matrix cracking and another criterion for possible delamination in the layers. In another study [25], impact resistance of composite laminates under low-velocity impact were studied by conducting drop-weight tests on various composite specimens. It was observed that delamination is the major failure in the seventh layer but fiber breakage is more important in the 13th layer. They concluded that in energy absorbing mechanism, number of layer is an important aspect in composite materials. Belingardi and Vadori [26] conducted low-velocity impact tests on unidirectional and woven glass- fiber-reinforced epoxy matrix laminates to study their impact behavior. They particularly analyzed two parameters, the degree of damage and the saturation impact energy in each test by changing the drop height. Milani and Yannacopoulos [27] presented two simplified models for out-of-plane impact response of composites. Clamping conditions, modes of bending, interlaminar failure, and effects of the mechanical properties of the material on strain rate were considered in their model. They made use of finite element approach and Hashin failure criterion to model the impact response of the structure. In other study, Naini and Babu [28]

studied initiation, propagation and modes of delamination in a pre-damaged stiffened laminate subjected to impact loading. In addition, they evaluated the effect of the delamination location on load carrying capacity of the stiffened plate. Their goal was to obtain the value of strain energy release rate in order to assess the crack initiation point for specific applied loads. Riccio *et al.* [29] numerically evaluated the behavior of laminated plains , stiffened with omega shaped stiffeners, under low velocity impact in different impact energies. Moreover, they simulated several damage models to understand the effects of intra-laminar and inter-laminar failures by using Hashin failure criterion and quadratic nominal stress criterion respectively. In their work, results of the full model and the model with only intra-laminar failure are approximately the same, which means the delamination had minor effects in the results. Chakraborty and Dutta [30] tried to find the optimum hybrid fiber-reinforced plastic plates subjected to impact loading in order to minimize the cost and weight of the laminate. Inter-laminar failure criteria were used in their optimization by evaluating potential matrix crack and delamination initiation. The number of lamina in the laminate, fiber directions, and lamina thickness were the variables during the optimization process. In another work, Young *et al.* [31] performed an optimization on a laminated composite subjected to impact loading by using a genetic algorithm to minimize the peak deflection and penetration. The variable of their work was fiber orientation of the plies. They checked intra-laminar failures to find the best result while ignored delamination initiation in their investigation.

1.2.4. Optimization of stiffened composite structures under impact loads

There are few studies on optimum design of stiffened composites. Thompson et al. [32]. optimized composite bridge deck panels to minimize the weight. The forces applied by vehicles passing over the panels are considered as impact loads. However, they did not carry out impact analysis; instead they modeled the impact load as a statically equivalent load. Jadhav and Mantena [33] attempted to increase impact energy absorption of grid-stiffened composite panels. However, they just performed a parametric study to improve impact resistance of the panel; they did not use an

optimization algorithm. Gigliotti *et al.* [34] minimized the weight of T-stiffened and I-stiffened composite panels subjected to impact loads. Local bucking and impact damage in the form of delamination were considered as constraints in the optimization problem. They applied a force statically to the center of the panel in their model to simplify the problem, and assumed that the buckling load level and the strain energy at the onset of delamination would be the same if impact loads were applied.

1.3. Problem Statement

Designing continuous fiber-reinforced composite structures against impact loading poses difficulties due to their brittle nature. A thin plate undergoes large deflection under impact forces resulting in large strains exceeding their limiting values. If the plate is designed as thick, it may become so stiff that its energy absorbing capacity in the form of strain energy of deformation becomes very small in the elastic range. In either case, the structural integrity of the composite structure may easily be lost unlike ductile metal structures. In the literature, stiffeners were mostly designed to make a composite plate stiffer in order to improve its buckling strength or its vibration properties. In this study, stiffeners are designed not to make the plate stiffer, but to introduce additional deformation mechanisms resulting in improved impact performance. The aim is to increase the impact resistance of composite plates with minimum use of material by optimally designing the stiffener. As the literature survey shows, there is no study on the design optimization of stiffened composites under real impact loading conditions. In this study, a generic problem is considered. A rectangular composite plate supported at its sides is subjected to collision impact. A hat-stiffener is bonded to the plate. A rigid impactor with a certain mass and velocity may hit the plate at various locations on the unstiffened surface (Figure 1.2). The objective function to be minimized is the weight of the stiffener. There are three design requirements: The maximum deflection should not exceed a limiting value. The structure should be able to absorb the impact energy without sustaining damage. Damage may occur due to intra-laminar failure like fiber breakage and matrix damage, or due to inter-laminar failure mechanism, which is delamination. Optimization variables are the dimensions of the stiffener, the width,

w_c, and height of the cap, h, width of the flange, w_f, and total width,w_s, and length, l, of the stiffener as shown in Figure 1.3. Thickness of the layers in the plate and the stiffener and the ply-orientation angles are taken as constant.

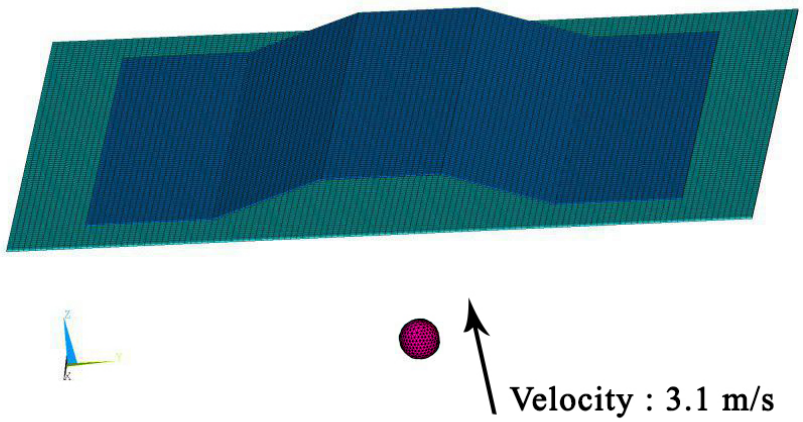

Figure 1.2. A stiffened plate under impact loading.

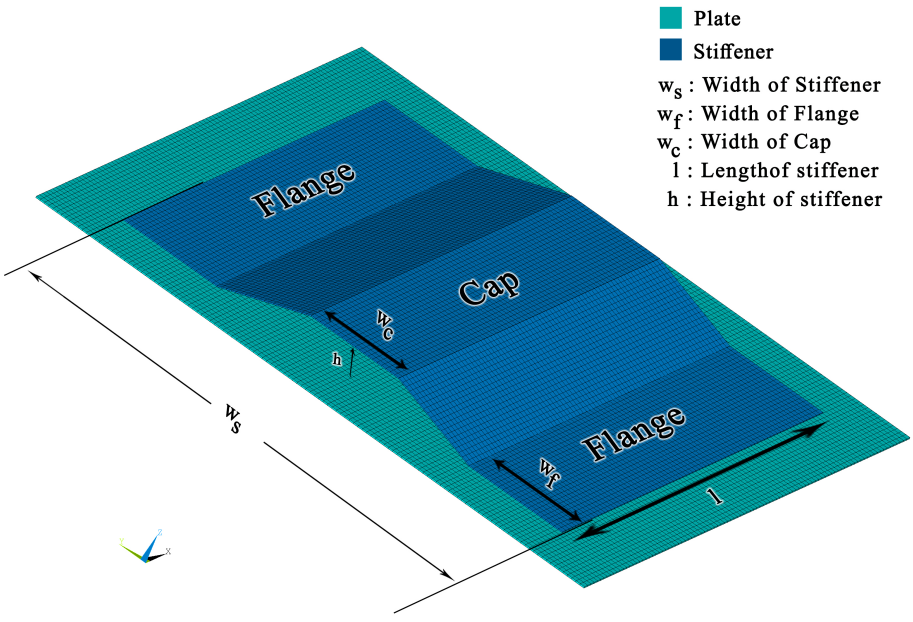

Figure 1.3. A hat-type stiffened plate.

The mechanical response of the stiffened plate under collision impact is simulated by developing a finite element model based on explicit formulations. For this purpose, ANSYS/LS-DYNA is used. The model is verified by comparing its predictions with the results of impact tests reported in the literature. The FE model is parameterized by defining the geometry and loading conditions in terms of parameters. The modified simulated annealing is used to find the optimum design. This is a global search algorithm that can start from an arbitrary configuration, search the entire solution domain, and find the globally optimal design or a near globally optimal design. Unlike deterministic local search algorithms, it does not easily get trapped in worse locally optimal points with proper implementation of the algorithm. Each configuration generated by the optimization algorithm is checked as to the satisfaction of the performance criteria. In order to check intra-laminar failure Tsai-Wu failure criterion is used. Hashin delamination initiation criterion is used to decide whether inter-laminar failure occurs. A code is developed using ANSYS parametric design language to implement the optimization algorithm and carry out structure analyses of configurations generated by the algorithm. Using the optimization procedure, optimal stiffener designs are obtained for different impact loading conditions. The optimal stiffened plates and unstiffened plates with different thicknesses are compared as to their weight, the maximum deflection, and the maximum failure index value.

2. THEORY

2.1. Composite materials failure

Variety of failure modes are observed in composite materials due to the anisotropic nature of these materials in response to either in-plane or out of plane loading. Main failure modes under in-plane loading are fiber tensile failure, fiber compressive failure, matrix tensile failure, matrix compressive failure, and shear mode failure (Figure 2.1) [35]. The most damaging in-plane failure mode is fiber breakage which occurs when the fibers cannot tolerate the applied loading. Impact loading is a major concern in composite structures. In addition, unlike metals where the impact damage is observed on their surface, in composites, damage may initiate from non- impacted surfaces. As a result, inter-laminar stresses should be considered as much important as intra-laminar failure modes. One of the important out-of-plane failures is delamination which happens when two adjacent plies separate leading to decrease in the strength and stiffness of the laminates [36]. Delamination can be the result of matrix cracks (Figure 2.2) [37] caused by high inter-laminar stresses due to commonly low through-thickness strength [38]. Several failure theories were proposed to predict failure in composite materials under different loading conditions. They can be categorized into two groups: in-plane and out-of-plane failure criteria. The most widely used failure criteria for composite materials are Tsai-Wu, maximum strain, maximum stress, Tsai-Hill, Hashin failure, and quadratic nominal stress criteria. To make use of the failure criteria, some material data should be known like X_t, X_c, Y_t and Y_c, which are tensile and compressive strengths along the fibers and transverse to fiber direction, respectively and S_{12},which is the shear strength. Some of these failure criteria are briefly introduced in this section.

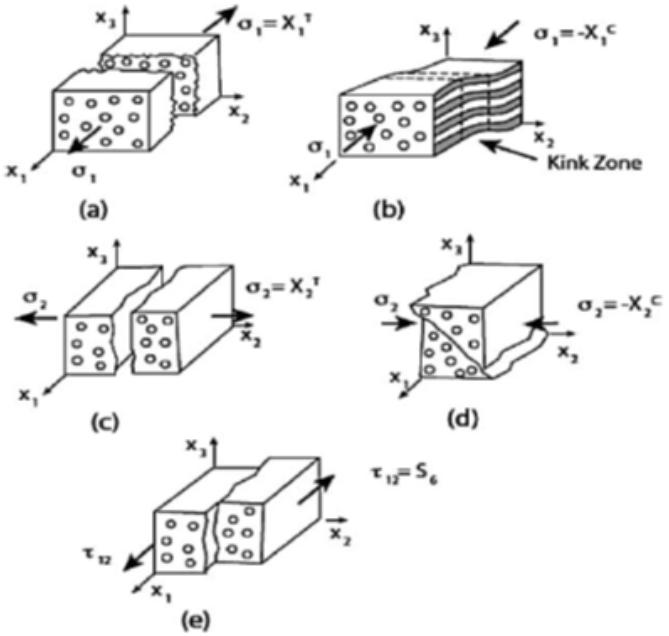

Figure 2.1. In-plane failure modes: a) Fiber tensile b) Fiber compressive c) Matrix tensile d) Matrix compressive e) Shear failure in the 1-2 plane [35].

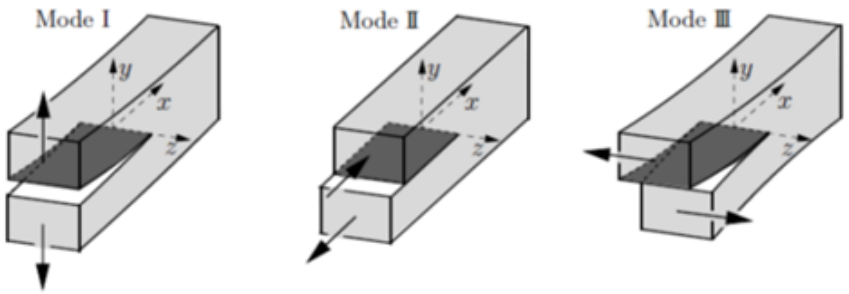

Figure 2.2. Crack opening modes [37].

Maximum stress criterion is a stress-based criterion and it can determine the failure mode. If one of the following equations is satisfied, failure occurs [1]:

Fiber failure:

$$X_t \leq \sigma_{11} \;\; or \;\; \sigma_{11} \leq X_c \tag{2.1}$$

Matrix failure:

$$Y_t \leq \sigma_{22} \;\; or \;\; \sigma_{22} \leq Y_c \tag{2.2}$$

Shear failure:

$$|\tau_{12}| \geq S_{12} \tag{2.3}$$

Maximum strain criterion is based on uniaxial failure strain and it specifies the failure mode. The failure initiates if one of the below conditions is satisfied [1]:

Fiber failure:

$$X_{\epsilon t} \leq \epsilon_{11} \, or \, \epsilon_{11} \leq X_{\epsilon c} \tag{2.4}$$

Matrix failure:

$$Y_{\epsilon t} \leq \epsilon_{22} \, or \, \epsilon_{22} \leq Y_{\epsilon c} \tag{2.5}$$

Shear failure:

$$|\epsilon_{12}| \geq S_{\epsilon} \tag{2.6}$$

where $X_{\epsilon t}$, $X_{\epsilon c}$, $Y_{\epsilon t}$, and $Y_{\epsilon c}$ are the maximum allowable tensile strains and maximum allowable compressive strains in the 1 and 2 directions and S_ϵ is the in plane failure shear strain.

Tsai-Hill failure criterion is a modification of von Mises criterion, which is usable for anisotropic materials. It is stress based and it does not specify failure mode. The equation for this criterion for plane-stress condition is [1]:

$$(\frac{\sigma_{11}}{X})^2 - \frac{\sigma_{11}\sigma_{22}}{X^2} + (\frac{\sigma_{22}}{Y})^2 + (\frac{\tau_{12}}{S_{12}})^2 \geq 1 \tag{2.7}$$

where X and Y are tensile or compressive longitudinal and transverse strengths respectively. Tsai-Wu failure criterion is a general form of Tsai-Hill criterion [1]:

$$\frac{\sigma_{11}^2}{X_t|X_c|} - \frac{\sigma_{11}\sigma_{22}}{\sqrt{X_t X_c Y_t Y_c}} + \frac{\sigma_{22}^2}{Y_t|Y_c|} + (\frac{1}{X_t} + \frac{1}{X_c})\sigma_{11} + (\frac{1}{Y_t} + \frac{1}{Y_c})\sigma_{22} + (\frac{\tau_{12}}{S_{12}})^2 \geq 1 \tag{2.8}$$

Hashin damage initiation is nonlinear and physically based criterion, which can indicate the failure mode. In plane stress condition, failure occurs when the following equations are satisfied [39]:

Fiber tension:

$$\frac{\sigma_{11}^2}{X_t^2} + (\frac{\tau_{12}}{S_{12}})^2 \geq 1 \quad if\ \sigma_{11} > 0 \tag{2.9}$$

Fiber compression:

$$\frac{\sigma_{11}}{X_c} \geq 1 \quad if\ \sigma_{11} < 0 \tag{2.10}$$

Matrix tension:

$$\frac{\sigma_{22}^2}{Y_t^2} + (\frac{\tau_{12}}{S_{12}})^2 \geq 1 \quad if\ \sigma_{22} > 0 \tag{2.11}$$

Matrix compression

$$(\frac{\sigma_{22}}{2S_{23}})^2 + [(\frac{Y_c}{2S_{23}})^2 - 1]\frac{\sigma_{22}}{Y_c} + (\frac{\tau_{12}}{S_{12}})^2 \geq 1 \quad if\ \sigma_{22} < 0 \tag{2.12}$$

where S_{23} is the shear strength in 2-3 plane. A failure theory based on the Hencky-von Mises energy theory was introduced by Norris. This theory is a nonlinear, stress-based and it can be implemented to predict failure behavior of orthotropic material. According to Norris failure criterion, if one of the following conditions is satisfied, failure occurs [40]:

$$(\frac{\sigma_{11}}{X})^2 + (\frac{\sigma_{22}}{Y})^2 - \frac{\sigma_{11}\sigma_{22}}{XY} + (\frac{\tau_{12}}{S_{12}})^2 \geq 1 \tag{2.13}$$

$$(\frac{\sigma_{11}}{X})^2 \geq 1 \tag{2.14}$$

$$(\frac{\sigma_{22}}{Y})^2 \geq 1 \tag{2.15}$$

Another failure criterion was presented by Chang and Chang [41]. This failure model shows the damage mode and damage occurs when one of the following equations is met:

$$(\frac{\sigma_{11}}{X_t})^2 + \beta(\frac{\tau_{12}}{S_{12}})^2 \geq 1 \quad if \quad \sigma_{11} > 0 \tag{2.16}$$

$$\frac{\sigma_{11}}{X_c} \geq 1 \quad if \quad \sigma_{11} < 0 \tag{2.17}$$

$$(\frac{\sigma_{22}}{Y_t})^2 + (\frac{\tau_{12}}{S_{12}})^2 \geq 1 \quad if\ \sigma_{22} > 0 \tag{2.18}$$

$$(\frac{\sigma_{22}}{2S_{23}})^2 + [(\frac{Y_c}{2S_{23}})^2 - 1]\frac{\sigma_{22}}{Y_c} + (\frac{\tau_{12}}{S_{12}})^2 \geq 1 \quad if\ \sigma_{22} < 0 \tag{2.19}$$

here, parameter β is the scale factor for shear stress. As it can be seen, if β=1, the criterion is similar to Hashin criterion and β=0 yields the maximum stress failure criterion. All of the discussed failure criteria account for intra-laminar failure modes and do not describe out-of-plane damage such as delamination. Hashin presented a delamination criterion in which delamination occurs if the following equation is satisfied [39]:

$$(\frac{\sigma_{33}}{Z})^2 + (\frac{\tau_{13}}{S_{13}})^2 + (\frac{\tau_{23}}{S_{23}})^2 \geq 1 \tag{2.20}$$

where S_{13} and S_{23} refer to out-of-plane shear strengths, σ_{33} and τ_{ij} are normal and shear stresses over the thickness of the considered ply, respectively. Z is the normal strength in thickness direction which is taken as:

$$if\ \sigma_{33} < 0 \ \rightarrow\ Z = Z_c\ and\ if\ \sigma_{33} > 0 \rightarrow\ Z = Z_t \tag{2.21}$$

Another failure criterion accounts for delamination initiation is proposed by Tsai [42]. Delamination occurs when the following equation is satisfied.

$$\frac{\sigma_1^2 + \sigma_{33}\sigma_{13}}{{X_t}^2} + (\frac{\sigma_3}{Z_t})^2 + (\frac{\tau_{23}}{S_{23}})^2 \geq 1 \tag{2.22}$$

2.2. Optimization algorithms

Optimization is a process which leads to finding the best design among all the feasible designs. An optimization problem has three parts. Objective function is the objective of the optimization and it should be minimized while the constrains of the

problem are not violated. The constrains give some limitations to the design. The value of the objective function in the optimization process depends on design variables. These variables are parameters which can be changed during the process but they may be also bounded in a predefined range due to the design restrictions. For better understanding there is an example; in design of a chassis of a vehicle which is made of composite materials, a design goal is finding the optimum impact resistance. Impact absorbent is the objective function which should be maximized but constraints which are buckling and strength limit the domain of the acceptable results. Variables of this problems can be angle of orientations of the fibers in the laminate which are limited between θ_1 and θ_2 degree.

After simulating the model, the first step to execute an optimization process is specifying proper constraints according to the type of loading, boundary conditions and the goal of the optimization. For example, the constraints can be local buckling, general buckling, deflection and strength. Then, the design variables should be specified and finally after choosing an appropriate optimization method due to the problem, the optimization procedure is performed.

Classical optimization methods like gradient methods and linear programming techniques are not practical in complicated problems. Because they may not be capable of finding the best solution resulting in calculating local optimum instead of global optimum. It is highly possible that a local optimum value deviates considerably from the global ones. So, in order to overcome these issues, some approaches were introduced such as simulated annealing (SA) and genetic algorithm (GA). Simulated annealing is a heuristic search algorithm to approximate the global optimum of an intended problem which by Kirkpatrick *et al.* [43] in 1983. SA is an efficient search method for large discrete search space and a reliable algorithm in finding the global optimum. It is inspired by solid materials annealing process, which involves a material heating until its temperature reaches melting point and slowly cooling them to crystallize their structures. Cooling should be in low pace because, at each temperature level, atoms of the material should be in the lowest energy so that the material keeps the equilibrium. The annealing process and decreasing the temperature continue till atoms form a crystal

with the lowest energy. Simulated annealing algorithm analogizes the annealing process such that lots of its configurations accord with the atoms placements, the cost function of a configuration accords with the energy of the atoms and the best result corresponds to the energy in crystal form. One of the principal concepts of SA algorithm is picking a random neighbor rather than the best one in every stage. If the result of this random neighbor is more satisfying, then it is the new next state, otherwise it will be the next state with probability of P (Metropolis probability) [44]. The probability gradually falls off to zero and results in finding the best global solution instead of the local one. Equation 2.23 represents this probability.

$$P\left(\Delta F\right) \, = \, e^{-\frac{\Delta F}{T}} \tag{2.23}$$

where ΔF shows the difference between the objective functions of the previous and current state and T represents the temperature of the simulated annealing process.

Simulating annealing algorithm have three important parts consisting [45] initial solution, objective function, and solution space. The solving process can be explained in three steps. In the first step, a random initial solution is generated which is the point that the SA algorithm iteration starts. In the second step, an initial temperature is specified. The assigned value should be high. The last step includes generating a new solution in a random neighborhood, obtaining the difference between the objective function with the previous iteration, calculating the probability P and decreasing the temperature. Figure 2.3 [44] shows the flow chart of the simulated annealing algorithm. In other words, in the simulated annealing, a starting point is chosen randomly and will be changed with a randomly generated point adjacent to the current configuration. Updating the initial point is an iterative process that ends when a stopping criterion is reached. As stated above, if the value of new cost function is smaller than the current one, the new point is replaced. If the new value is the larger one, the new point can be accepted according to the mentioned probability (P). This probability depends on the temperature. To prevent entrapping in a local optimum, the temperature should be reduced very slowly. By gradually decreasing the probability in the process, finally,

no local optimum (higher cost) is acceptable and the best solution is achieved.

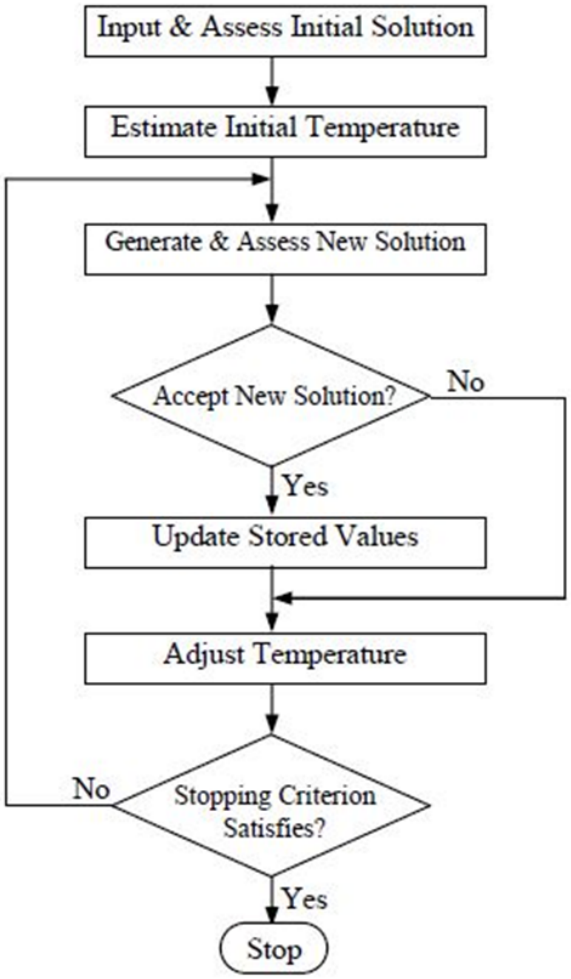

Figure 2.3. The procedure of SA algorithm [44].

Direct search simulated annealing (DSA) is a modified version of SA which was developed by M. Ali *et al.* [45] and improved by Akbulut and Sonmez [46]. The difference between DSA and SA algorithms is the use of a population of current configuration instead of a single one. The procedure of DSA is similar to the simulated annealing algorithm. Like simulated annealing algorithm, DSA is based on generating random configurations, acceptance probability and slowly reducing the temperature. The main modification is that the algorithm works with several configurations instead of only one configuration. It means that instead of searching one neighborhood, DSA searches the neighborhood of all current points. In the sets of current configurations, there is

certainly a point with the best result and one with worst result. In the process, the worst configuration is replaced with an accepted new generated configuration. So, all other configurations are kept including the best one. The iterations stop when the difference between the worst and the best value becomes small.

3. OPTIMIZATION PROCEDURE

3.1. Introduction

In this study, the stiffened composite plate is optimized by Modified Simulated Annealing Algorithm (MSA). The aim is to find the minimum weight of the structure while the strength and deflection are the constraints for the problem. The optimum stiffened plate should have the best impact resistance such that it tolerates failure and deflection should remain in an acceptable range. To evaluate the intra-laminar failure, Tsai-Wu failure criterion is used and to check the delamination, Hashin delamination initiation criterion is used.

3.2. Objective function

The objective function in this study includes weight, deflection and failure criteria. After solving the finite element model of the stiffened plate subjected to transverse static and impact loads, objective function value calculated for each configuration. Finding an accurate optimum shape requires having some restrictions and penalties in the objective function, so, the maximum deflection and the failure behavior of the stiffened plate added to the objective function in order to improve the effectiveness of the optimization process. The objective function used for the stiffened plate is:

$$\mathrm{F_{obj}} = \mathrm{C_1}\,\frac{\mathrm{W}}{\mathrm{W_i}} + \mathrm{C_2}\,\mathrm{P_{def}} + \mathrm{C_3}\mathrm{P_{TW}} + \mathrm{C_4}\mathrm{P_H} \tag{3.1}$$

where W and W_i are the current and initial weight of the stiffened plate, respectively, C_is are the weighting coefficients, P_{def}, P_{TW} and P_H are the penalty functions. P_{def} is defined as below:

$$\mathrm{P_{def}} = \langle \delta\mathrm{max} - \delta\mathrm{acc} \rangle^2 \tag{3.2}$$

where $\langle \delta \text{max} - \delta \text{acc} \rangle$ expressed as below :

$$\langle \delta max - \delta acc \rangle = \begin{cases} 0 & , \ \delta max < \delta acc \\ \\ \frac{\delta max}{\delta acc} - 1 & , \ \delta max \geq \delta acc \end{cases} \tag{3.3}$$

The deflection of the stiffened plate should be lower than an acceptable value, so this penalty function ignores the stiffened plates with large deflection.

The second penalty function, P_{TW}, is used in order to check the intralaminar failure. The Tsai-Wu failure penalty calculated as shown in Equation 3.4:

$$\text{P}_{\text{TW}} = \langle \text{F}_{\text{TW}} - 1 \rangle^2 \tag{3.4}$$

where $\langle \text{F}_{\text{TW}} - 1 \rangle$ expressed as Equation 3.5 :

$$\langle F_{TW} - 1 \rangle = \begin{cases} 0 & , \ F_{TW} < 1 \\ \\ F_{TW} - 1 & , \ F_{TW} \geq 1 \end{cases} \tag{3.5}$$

where, F_{TW} is the Tsai-Wu value in each configuration. According to its penalty, if the value of the Tsai-Wu is greater than one, it adds penalty to the objective function. In contrast, if the value of the Tsai-Wu is less than one, it means that there is no failure in the plate so the objective function value will be calculated without Tsai-Wu penalty.

The third penalty function, P_H, is used to predict delamination initiation. The penalty function P_H exactly works like F_{TW}, if the Hashin failure criterion value is greater than one, it adds penalty to the objective function.

To find the proper weighting coefficients, a process of trial and error is performed. Several stiffened plates with different dimensions of stiffener are modeled and maximum

deflection, Tsai-wu and Hashin delamination initiation values are obtained for each case. It is observed that the only critical parameter in the objective function is intra-laminar failure criterion and delamination does not occur. In addition, the maximum deflection is less than the acceptable value even in the worst case. As a result, the penalty functions for deflection and delamination are not activated and the values of their weighting coefficients do not affect the objective function. However, because the structure can not resist intra-laminar failure in some cases, a large weighting coefficient for Tsai-Wu penalty function is chosen.

3.3. Modified Simulated Annealing (MSA)

The optimum design of the stiffened plate is achieved using Modified Simulated Annealing (MSA). The cross sectional shape of the stiffened plate is defined by lines passing through key points. x, y and z coordinates of the moving key points are selected as design variable of this optimization algorithm. In this study there are three moving key points where, x coordinate of all of them is the same and z coordinate for two key points is always zero. So, the number of restricted degrees of freedom is 4. As there is 9 degrees of freedom totally, the number of design variable is 5:

$$n = 5 \tag{3.6}$$

where n is the number of design variables in this study. Changing the position of the key points leads to generate a new shape, where the position of the x, y and z coordinates of the new shape is obtained by summing up the current value of the key points with a random directional value. X_{kf}, Y_{kf} and Z_{kf} are the coordinates of the K_{th} moving key point of new configuration as:

$$\mathrm{X_{kf}} = \mathrm{X_k} + \mathrm{C_{rand}R_x} \tag{3.7}$$

$$\mathrm{Y_{kf}} = \mathrm{Y_k} + \mathrm{C_{rand}R_y} \tag{3.8}$$

$$\mathrm{Z_{kf}} = \mathrm{Z_k} + \mathrm{C_{rand}R_z} \tag{3.9}$$

where, X_k, Y_k and Z_k are coordinates of the K_{th} key points of currently generated shape, C_{rand} randomly generates series of numbers in the range of (-1,1), R_x, R_y and R_z indicate the available maximum distance that each KP can move which is different in each direction. According to the search domain in this study, the values of newly generated key points depend on the previous key points. The accuracy of the shape optimization depends on the number of the design variables. At the first stages of the optimization, certain shapes are generated by randomly generated values for x, y and z coordinates. The number of these initial configurations depend on the number of the design variables which is called N_{Conf} in this study.

$$\mathbf{N_{Conf}} = 9\mathbf{n} \tag{3.10}$$

Unlike the standard Simulated Annealing (SA), this algorithm generates a new set of configuration in each iteration. The objective function value for each generated configuration is calculated after solving the finite element model. Then, by comparing the highest objective function value of newly generated configuration to current one at each iteration, its acceptability is evaluated according to the following convention: If F_{obj} is less than or equal to F_h (highest objective function value of a current configuration), it will be accepted but on the other hand, if F_{obj} is greater than F_h the acceptability of the configuration depends on the following expression:

$$\exp\left(\frac{F_h - F_{obj}}{T_k}\right) \tag{3.11}$$

If a new configuration has a lower objective function value than F_h, it is accepted. Otherwise, acceptance of the configuration depends on the aforementioned acceptability convention, which after calculating its value, it will be compared with a randomly generated number between 0.0 and 1.0. If the value is higher or equal to the random number, it is accepted and vice-versa. The accepted configuration from the previous stage is replaced with a point lower than the worse point. Thus, the configurations which are located between the best and worse points remain in the current configuration.

The acceptance of the probability is controlled by using temperature parameter, T_k. At the first stages of the optimization process, the value of the T_0 has its own high values to accept all configurations regardless of its objective function value. By selecting a high value for temperature at the beginning, the algorithm searches the whole domain. The group of configurations that are generated under a constant temperature is called Markov Chain. Minimum length of Markov chain depends on the number of design variables:

$$Lt = 3n \tag{3.12}$$

As could be seen in Equation 3.13, the length of the current Markov chain depends on the step size ratio which indicates that as the step size ratio goes to 0, the length of the current Markov chain is two times of Lt or remains same, otherwise it gets tripled.

$$Lt_c = \text{nint}\left(\text{Lt}\left(1 + 2\left(\frac{\text{rs}}{\text{rs}_{\text{in}}}\right)\right)\right) \tag{3.13}$$

where Lt_c is the length of the current Markov chain, *nint* is an APDL command which finds nearest integer to the value within the parentheses, rs and rs_{in} are the current and initial step size, respectively. The selection of the initial step size depends on the search domain and behaviour of keypoints' movement. If the F_{obj} is less than the best configuration into the inner loop, it replaces the best point. Then the current

loop closes and a new one starts.

$$Lt_n = in \tag{3.14}$$

in which Lt_n is newly accepted Markov chain. and "in" is the Markov chain iteration. The number of the improvement increases using following equation:

$$N_{im} = N_{im} + 1 \tag{3.15}$$

where N_{im} is the number of improved configuration found into the inner loop. Otherwise, if no improvement occurs in the worse configuration then the step size "rs" reduces such that:

$$rs = 0.9rs \tag{3.16}$$

In final stage of Markov chain, the temperature will decrease using following criterion:

$$R_a = \frac{A_m}{in} \tag{3.17}$$

in which, R_a is the ratio of the accepted movements and A_m is the number of the accepted point.

$$R_s = (\frac{rs}{rs_{in}}) + 0.01 \tag{3.18}$$

that R_s is the step size ratio,

$$\begin{cases} \alpha = \alpha_{min} & if\ R_a > R_s \\ \alpha = \alpha_{max} & if\ R_a < R_s \end{cases} \tag{3.19}$$

where, α is the decrement constant for the temperature and α_{min} and α_{max} are 0.9 and 0.9999, respectively. At the end, the worse and the best configurations will be compared. If the current temperature is less than the tolerance "epsin=5e-04", then the difference of the worse and the best configuration should be less than "epsinout=5e-08" to finish the optimization, otherwise the temperature will be decreased to be less than "epsin" as follow:

$$ck = alpha * ck \tag{3.20}$$

4. NUMERICAL SIMULATION

Since most of the experimental analyses such as drop test are destructive and expensive, Finite element method (FEM) is a preferable and efficient way of analyzing structural behavior. In addition, some information cannot be obtained by experimental tests and should be simulated numerically. For example, in composite materials, numerical study of intra-laminar failures may not be as challenging as experimental study. Moreover, the only way to get the optimum result in optimization problems is to develop a parametric numerical model. In this study, the model is developed by ANSYS Mechanical APDL (ANSYS parametric design language) which is a powerful and reliable commercial finite element software. The most important steps to simulate a model:

- Specifying the loading type
- Choosing proper element types
- Defining suitable material models
- Modeling parametrically when the model will be optimized
- Generating FE mesh
- Defining contacts when it is needed
- Applying boundary conditions

Loading can be either static or dynamic such as impact and crash. In static analysis, mass or damping does not affect the solution, unlike dynamic analysis which is time-dependent and nodal forces are related to the mass. There are two types of approaches to solve a finite element problem: static analysis (Equation 4.1) and dynamic analysis (Equation 4.2) [47].

$$[K]\{u\} = \{F(t)\} \tag{4.1}$$

$$[\mathrm{M}]\{\frac{\mathrm{d}^2\mathrm{u}}{\mathrm{dt}^2}\} + [\mathrm{C}]\{\frac{\mathrm{du}}{\mathrm{dt}}\} + [\mathrm{K}]\{\mathrm{u}\} = \{\mathrm{F(t)}\} \tag{4.2}$$

where [K], [M] and [C] are system stiffness, system mass and system damping coefficient matrices respectively and u, $\frac{du}{dt}$, $\frac{d^2u}{dt^2}$ and F indicate displacement, velocity, acceleration, and applied loads, respectively. According to Equation 4.1, when the loads are known, the displacements can be calculated by inverting the stiffness matrix. This approach can be used to analyze the problems in which time is not a major factor such as static and modal problems.

On the other hand, as it is seen in Equation 4.2, the displacement is a function of time and it can be used to solve dynamic problems. For solving motion equation, implicit methods and explicit methods can be used. The implicit methods have more stable characteristics but it should be mentioned that inversion of stiffness matrix leads to higher computational costs. The explicit methods can avoid the stiffness matrix inversion because of the presence of the mass matrix. Moreover, in the nonlinear implicit analysis, several iterations are requisite to achieve equilibrium in each solution step. However, in the explicit method, results are obtained without any iteration and consequently, this process is taking less time than the implicit analysis. To overcome the stability problem in the explicit analysis, the time step is limited, and the minimum time step is estimated by using finite element software. In this study, the stiffened plate that is subjected to static loading is modeled using an implicit solver in ANSYS/MECHANICAL. In another case, when the laminated stiffened plate is under impact loading, the model is simulated by explicit ANSYS/LS-DYNA.

In the stiffened plate, the plate is constrained in lateral ends so that it is fixed with zero degrees of freedom (Figure 4.1).

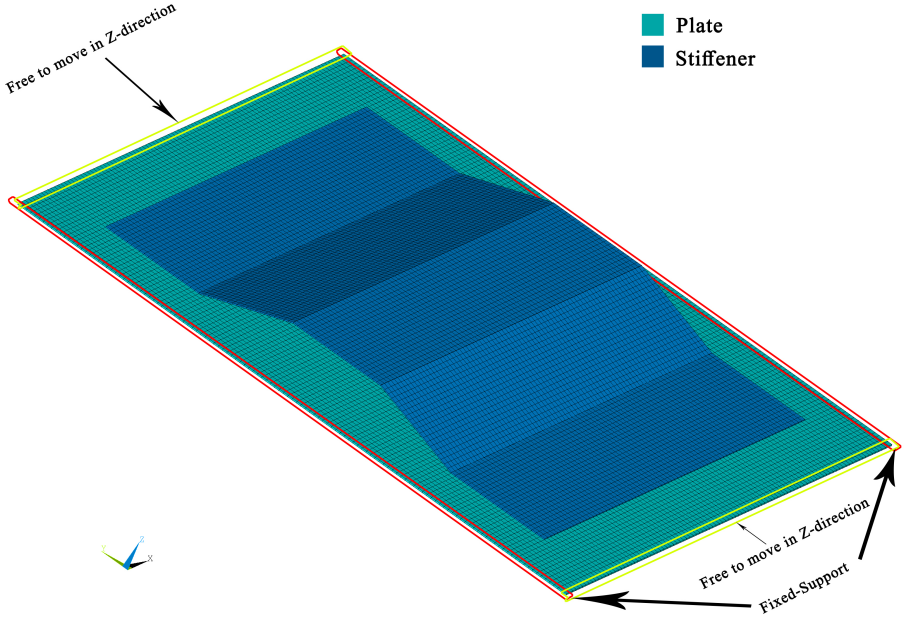

Figure 4.1. Boundary conditions of the stiffened plates.

4.1. FEA of laminated stiffened plate (Static Loading)

In order to evaluate the effects of adding a stiffener to a plate, it is necessary to simulate the stiffened plate and the plate without stiffener. Both of these models are subjected to a transverse force with a magnitude of 700 N and this force is distributed to an area with dimensions of 28 mm×28 mm at the center of the plate (Figure 4.2).

After creating the areas, assigning the material properties, and specifying layups of the composite material, the next step is to generate the finite element meshes. Selecting a suitable element type is crucial. Shell elements are practical in the modeling of many composite structures where the thickness of the structure is much smaller than length and width of it. These elements are very efficient in computational cost because the number of finite elements is much less than the solid elements. Shell 181 is the proper element type for this work. It can be used in shell structures with thin to medium thicknesses, large rotation and large strain nonlinear applications for

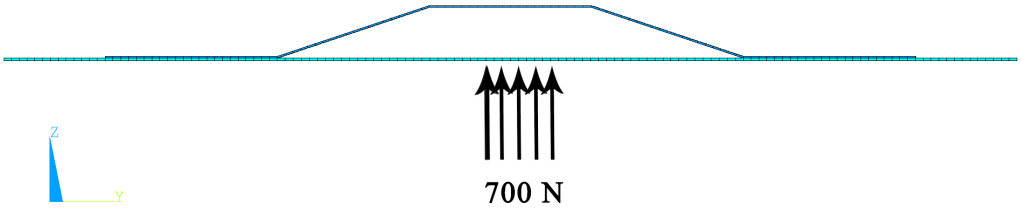

Figure 4.2. The stiffened plate under static loading.

modeling layered composite shells [48]. As it is seen in Figure 4.3, this element is formed by four nodes and has a translational degree of freedom in x, y and z directions and a rotational degree of freedom about them as well. I, J, K and L represents the nodes of the element. In the Figure 3.3, x_0, y_0 and z_0 axes indicate element coordinate system when the element orientation is not defined while x, y and z axes show the specified element coordinate system with the orientation of the element is given.

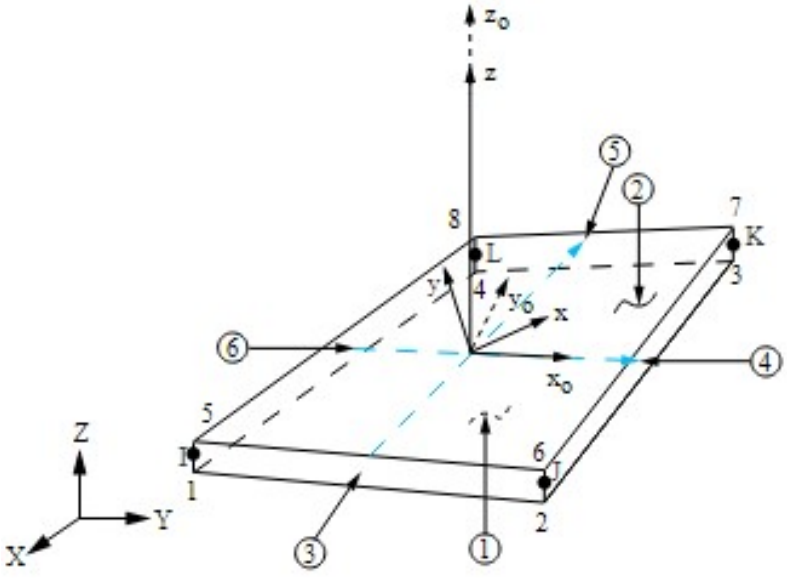

Figure 4.3. Shell 181 geometry [48].

After meshing, the stiffener part and the plate should be attached together. This is done by using target and contact elements. Among the ones that ANSYS provides, CONTA175 and TARGE170 are chosen (Figure 4.4) [48]. The contact element is placed on the surface of the shell elements of the stiffener and bonds with the target element located on the surface of the shell elements of the plate. Although this connection can be permanent, the separation between contact and target may occur. This potential separation simulates the interface delamination. To correctly model the contact and the target, outward normal of the target surface should point toward the contact surface (node).

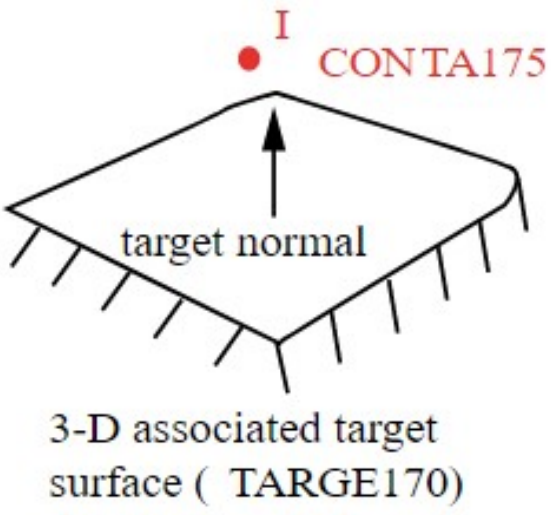

Figure 4.4. Contact and target elements geometries [48].

4.2. FEA of laminated stiffened plate (Impact Loading)

In this section, a stiffened composite plate and a plate without stiffener subjected to low velocity impact are modeled in ANSYS/LS-DYNA. After creating key points, lines and areas, proper material model for the composite structures is chosen. The composite damage model Chang and Chang, which is a nonlinear inelastic model, is used to predict intralaminar failure. Use of the composite damage model requires the mechanical properties such as elastic modules and Poisson's ratios, laminate strengths in material directions, bulk modulus in compressive failure, and nonlinear shear stress

parameter. Shell elements are chosen for generating finite element meshes for modeling the stiffener and the plate. Shell163 is the only shell element that is provided by the software for explicit analysis. There are four nodes in the element with 6 degrees of freedom at each node. These degrees of freedom are translation in the x, y and z-axes directions and rotation about those axes. Figure 3.5 [49] shows the geometry and nodes placements in shell 163, nodes are named as I, J, K and L.

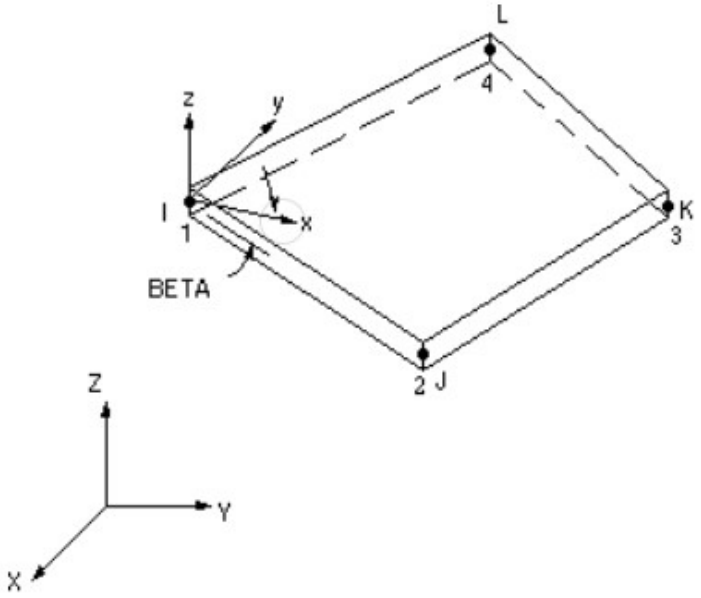

Figure 4.5. Shell 163 element [49].

By selecting the composite option in this element, the fiber orientation of each layer is defined. The number of the integration points should be defined through the thickness. If the given number is the same with the number of layers, each integration point is placed in the middle of the layer. In this study, it is taken as the same as the number of layers for the plate and the stiffener.

To simulate the stiffened plate model, tie-break surface-to-surface contact (TSTS) is defined in order to attach the stiffener part and the plate part together. This contact type will be explained in the next section in detail. Another contact should be specified between the impactor and the plate. Automatic surface-to-surface contact (ASTS) is

chosen in this study so that the impactor and the plate are defined as the contact part and the target part respectively. Automatic contact types are recommended for many applications because their search algorithm is very fast and the orientation of the contact surface of the shell elements are determined automatically. Surface-to-surface contact is used when the surface of a body contacts the surface of other body and this is preferred when the contact area between the two bodies is not too small.

The impactor is modeled as a body with a hemispherical shape and the mechanical properties of Aluminum. However, the effect of the deformation of the impactor is not considered in the study, it is defined as a rigid body. Finite element meshes are generated using a solid element. Figure 4.6 shows the FE model of the stiffened plate.

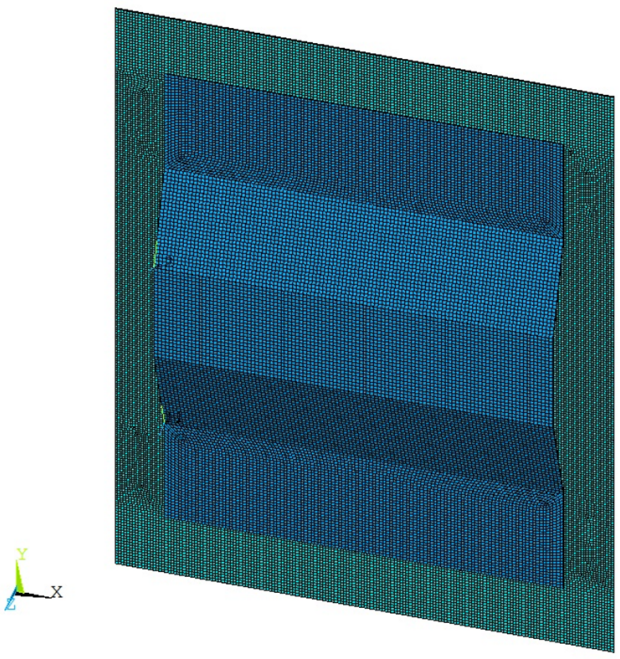

Figure 4.6. The FE model of the stiffened plate.

4.3. Delamination modeling

In high velocity impacts, matrix cracks are created as a result of high impact energy resulting in delamination. Delamination decreases the stiffness of the composite material gradually during the impact loading. On the other hand, when the initial kinetic energy is a low, delamination failure may not happen [50]. In this study, the delamination failure is checked for each newly generated configuration. In addition, the goal of this study is to find the lightest stiffener such that any failure will not be observed. Because no delamination is allowed in the optimum structure as a design constraint, analyzing progressive damage and damage area is not needed and only delamination initiation is checked.

In the composite damage model based on Chang-Chang failure criterion, only intra-laminar failures are considered. So, a method should be utilized to model delamination. There are few methods to check or model delamination in composite materials. If only delamination initiation is considered, a single composite shell is enough to predict delamination. In this case, instead of defining integration points only at the centers of the layers, as it is seen in Figure 4.7 [51], additional integration points should be defined at the interfaces. Besides, properties of the epoxy resin as well as the composite plies need to be defined. The thickness of the interfaces between the layers is much less

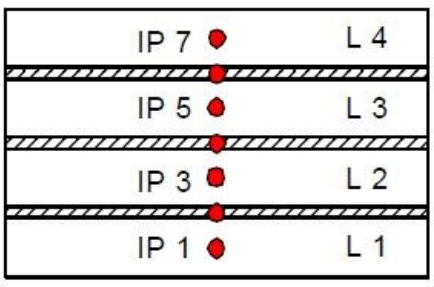

Figure 4.7. Integration points indicating layers and interfaces [51].

than the thickness of the plies. Moreover, the material used for the interfaces is epoxy while the material used for plies is glass- fiber-reinforced epoxy composite. Three more

parameters need to be defined to model the shell layups:

- Weighting factor (WF(i)) which is the thickness corresponding to each integration point divided by the total thickness.
- Material ID for each integration point. Mechanical properties and strengths of the epoxy resin is shown in Table 4.1 [52].
- Integration points coordinates (S(i)) in the range of -1 and 1 (Figure 4.8) [49].

In this study, since the plate is made of 20 layers, there are 19 interfaces. So, 39 integration points are defined in order to check whether delamination occurs or not. Delamination happens when either transverse shear stress in a ply reaches its maximum or the delamination failure criterion is met.

Table 4.1. Mechanical properties and strengths of the epoxy resin [52].

Parameters	**Values**
$Elastic Modulus, E\ (GPa)$	3.2
$Poisson's Ratio, \nu\ (-)$	0.278
$Shear Modulus, G\ (GPa)$	1.2
$Tensile Strength\ (MPa)$	85
$Compressive Strength\ (MPa)$	120
$In-plane Shear Strength\ (MPa)$	114
$Density\ (Kg/m^3)$	1200

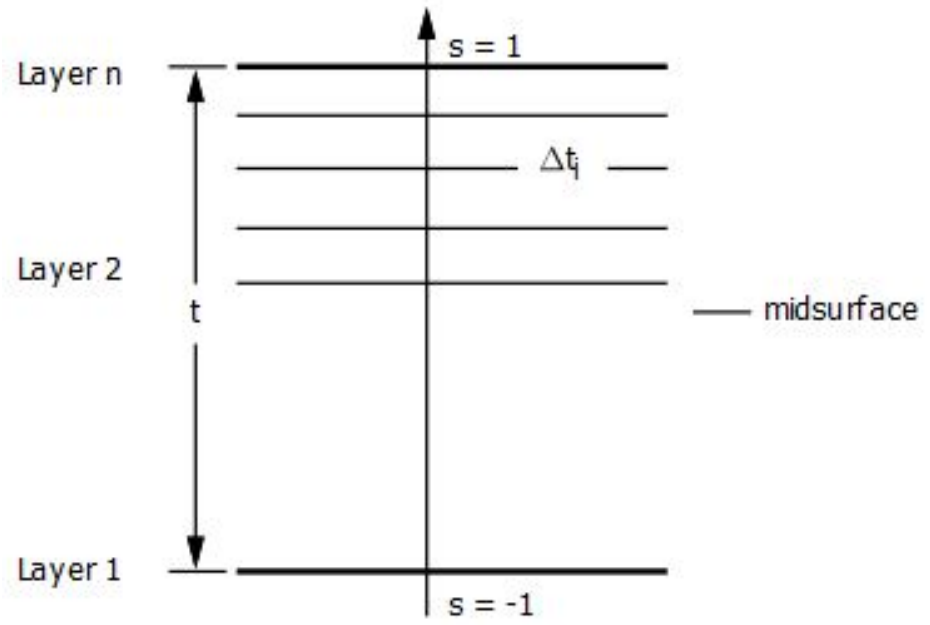

Figure 4.8. Ordering of the integration points [49].

If delamination initiation and propagation in low velocity impact need to be determined, the proposed method by ANSYS explicit would be tiebreak contact model. In this method, instead of modeling a single shell, several composite shells are simulated depending on how many interfaces are going to be evaluated. The tiebreak contact makes a contact between the interfaces of two shells. The tiebreak contact model is based on cohesive element formulation however it does not create cohesive elements. In the automatic surface-to-surface tiebreak contact (ASTS), which is used in this study and also in the verification, the contact model works properly. Therefore first, the tiebreak contact ties the interfaces of two shells, and then during the impact, if the out-of-plane shear and normal stresses exceed their limiting values, delamination occurs [49]. In this study, delamination initiation is evaluated by the failure criteria proposed in reference [39] and ASTS contact model is used only for attaching the stiffener part and the plate together.

5. MODEL VERIFICATION

The model developed in the present study is validated by comparing its results with the results of two different experimental studies on low-velocity impact response of composite materials. Heimbs *et al.* [53] investigated impact on simple composite plates. Numerical simulation was performed in their work as well as experimental tests in order to study the factors that influenced the impact performance. Greenhalgh *et al.* [54] conducted an experimental study to investigate damage characteristics of a stiffened composite plate subjected to low-velocity impact. The models are explained in the following sections and mesh convergence analysis is carried out for the simulation model of the stiffened laminated plate to be optimized.

5.1. Verification using the experimental results reported by Heimbs *et al.* [53]

Heimbs *et al.* [53] carried out an investigation, both experimentally and numerically, about low-velocity impact on composite plates. Their aim was to evaluate the effect of compressive preloads on carbon fiber-reinforced epoxy (CFRP) plates by conducting several impact tests on preloaded and unloaded specimens and also by simulating low-velocity impact using commercial FE code LS-DYNA. Here, the results of the impact tests on unloaded plates are used in the verification of the present model.

Three different CFRP plates with different stacking sequence and manufacturing process were investigated. Mechanical properties of using materials were given in Table 5.1. They are defined as follows:

Type A: Non-crimp fabric (NCF) in a symmetric, quasi-isotropic lay-up with 24 plies with total thickness of 3.2 mm.

Type B: Prepreg tape in a symmetric, quasi-isotropic lay-up with 24 plies with total thickness of 2.7mm.

Type C: Prepreg tape in a symmetric lay-up with preferred zero degree of fiber direction and 24 plies with total thickness of 2.7 mm.

The stacking sequence of type A and B is $[-45/0/+45/90]_{3s}$ and the stacking sequence of type C is $[0/+45/0/-45/0/0/+45/0/-45/90/90/0]_s$.

Length of the plates was 400 mm and width of them was 150 mm but after bonding both sides of them with 2 mm thick and 50 mm width tapered GFRP tabs, free length of the plates was decreased to 300 mm (Figure 5.1). Six strain gauges were applied to the plates which give information about uniform load distribution and possible buckling under preload.

Table 5.1. Mechanical properties of the CFRP laminates [53].

Parameters	**Type A**	**Type B,C**
E_1 (GPa)	124	153
E_2 (GPa)	10.5	10.3
G_{12} (GPa)	4.2	5.2
ν_{12} $(-)$	0.3	0.3
X_t (MPa)	1953	2540
X_c (MPa)	1378	1500
Y_t (MPa)	67	82
Y_c (MPa)	240	236
SC (MPa)	61	90

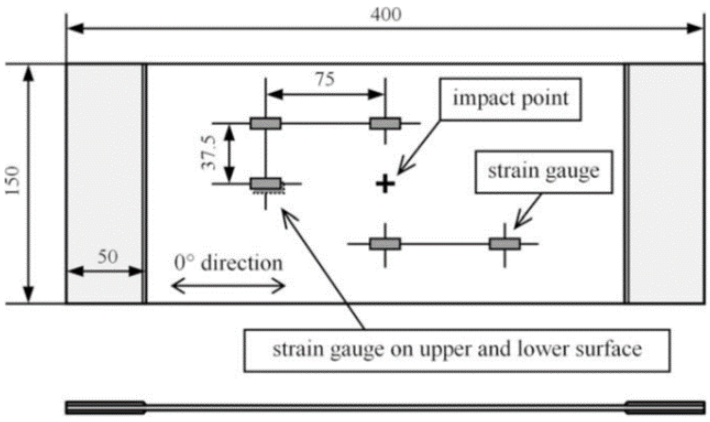

Figure 5.1. Dimension of specimens (dimensions are in mm) [53].

S.Heimbs conducted the low velocity test on a Dynatup 8250 drop tower facility (Figure 5.2).

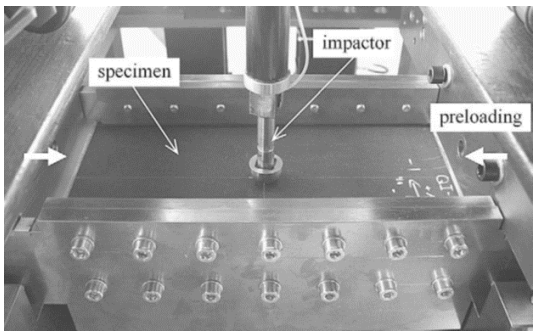

Figure 5.2. Top view of the specimen fixture and the impactor [53].

5.1.1. Boundary conditions and low velocity impact details

The specimen had fixed support in longitudinal ends using two clamping jaws and simply support in lateral ends which allowed rotations during the impact loading (Figure 5.3).

A hemispherical steel impactor with a mass of 1.85 kg and a diameter of 25.4 mm was used in all the tests. The impact energy has constant value about 40 J.

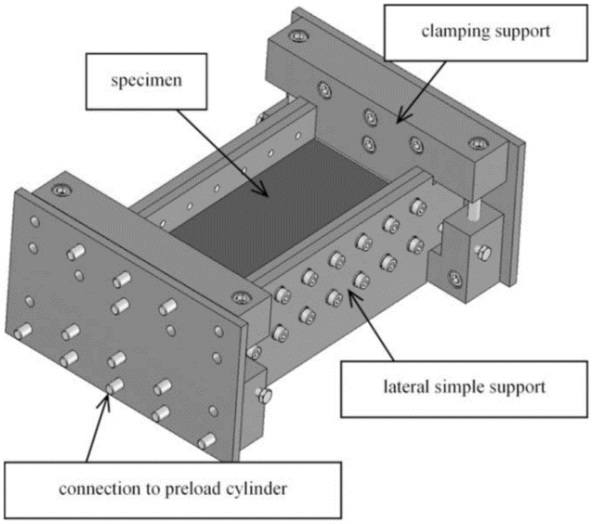

Figure 5.3. Fixture of the plates [53].

5.1.2. Modeling and simulation

Heimbs *et al.* [53] simulated the impact loading using LS-DYNA software to evaluate inter-laminar (delamination) and intra-laminar failure of the composite plates. To model the composite plates, they used shell elements with 2D modeling approach and chose the linear-elastic composite model Mat54 based on Chang - Chang failure model. They used layered shell modeling approach in their study in which each integration point represented one single layer. Moreover, a spherical rigid body using shell elements and material model Mat20 was modeled as the impactor. Since the implemented failure model did not include delamination failure, they used LS-DYNA contact formulation, automatic one-way-surface-to–surface tiebreak, to consider delamination in the simulation model. They simulated different models with two, three, four, and six shells with a total number of 24 layers in which each shell includes several layers. For each model tiebreak contacts were defined between the shells. In addition, they simulated the plate with only one shell and no tiebreak contact to investigate the effect of the delamination on the results.

In the current study, a model is developed to simulate the low velocity impact on the plate by using finite element commercial program ANSYS/LS-DYNA. The geometries, the material types, and the boundary conditions are the same as the experiment.

By using composite damage model and inputting elastic modulus, shear modulus, and Poisson's ratio, elastic behavior of the plate is obtained. Because the thickness of the plate is insignificant compared to its length and width, shell elements with the formulation of Belytschko-Tsai are chosen. The impactor is defined as a solid spherical steel rigid body.

Two contact types are determined for the simulation; automatic surface-to-surface and tiebreak surface-to-surface. First one is defined to model the contact between the impactor and the plate and the second one is used to model the inter-laminar failure. Since this contact type cannot be defined between the layers of a single shell, more than one shell should be specified, and the tiebreak contacts are defined between the interfaces of the shells.

5.1.3. Comparison of ANSYS/ LS-DYNA results with Heimbs' experimental and numerical results

In the model developed for low-velocity impact, the impactor with a mass of 1.85 kg is dropped on the plate. The velocity of impact is 6.5 m/s resulting in 40 J impact energy. The impact response is investigated in two cases. Delamination is ignored in the first case and in the second case it is modeled. Figure 5.4 and Figure 5.5 show the contour plot of the displacements when the plate experiences the maximum deflection. In the first figure, only one shell with a total thickness of 2.7 mm and 24 layers is modeled so, inter-laminar failure is not considered. In the second figure, three shells are modeled to simulate delamination. The thickness and the number of layers are the same in each layer and they are equal to 0.9 mm and eight layers, respectively. Their interfaces are in contact by using tiebreak surface-to-surface contact.

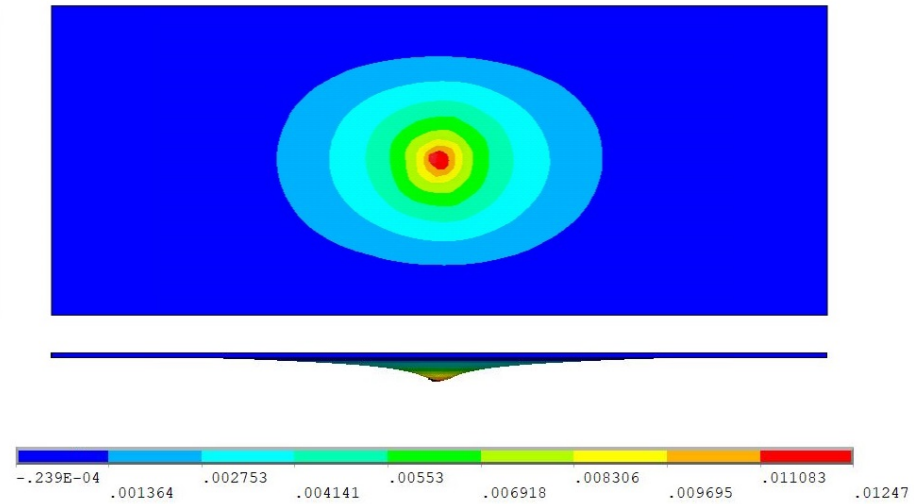

Figure 5.4. Deformation plot of the plate when delamination is ignored.

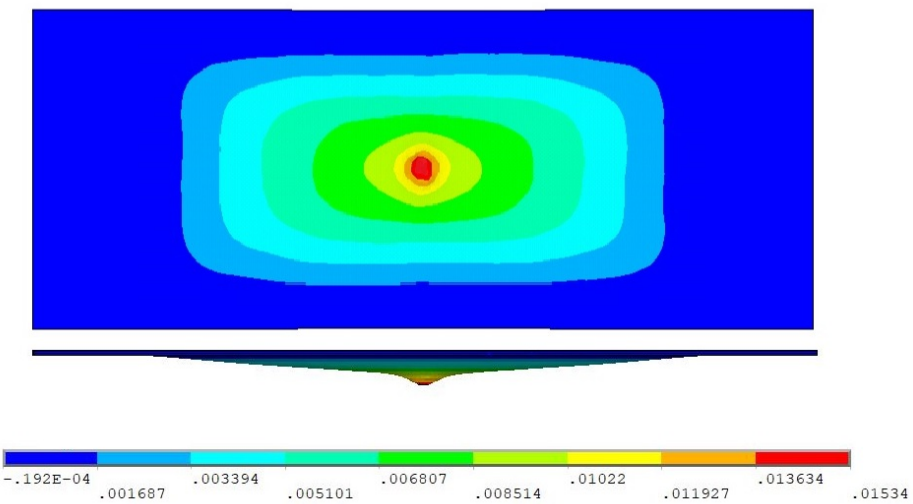

Figure 5.5. Deformation plot of the plate when delamination is considered.

The maximum deflection of the plate in the experiment is 12.2 mm and as it can be seen in Figure 5.4, it is 12.3 mm in the simulation; thus there is a perfect agreement between the results. However, by using tiebreak contacts, the result is 15.3 mm, which is 3 mm larger than the experimental result. This is because the bending stiffness decreases due to tiebreak contacts. It is observed that by using more than one shell

to model the plate, whether delamination occurs or not, the plate bending stiffness decreases; consequently, the maximum deflection increases.

Figure 5.6 demonstrates the graphs of contact force on the plate obtained numerically using three- shell model and reported by the experimental study, as it can be seen there is a good agreement between the experimental result and the FE model.

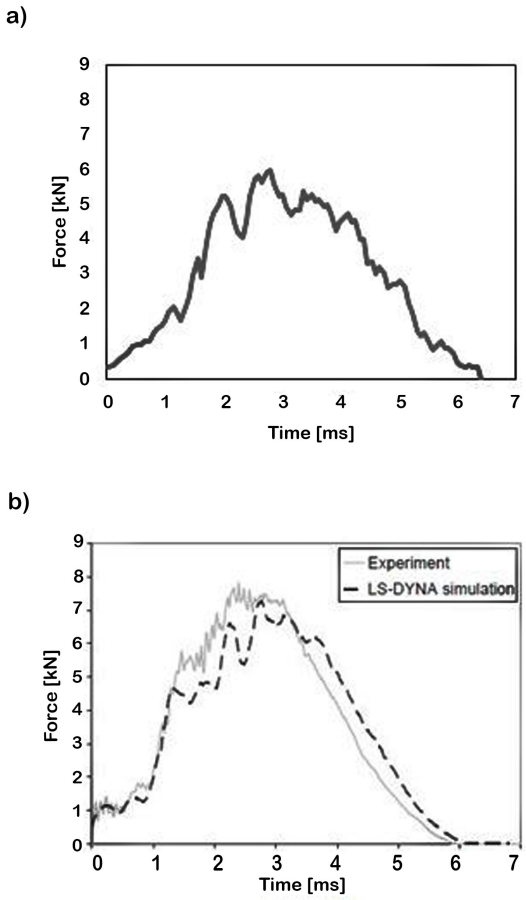

Figure 5.6. Contact force plots: (a) plate made of three shells (delamination included) (b) Heimbs results [53].

According to the contact force plots, it is observed that, using tiebreak contacts give better results in comparison with using only one shell to model the plate. It shows that delamination is the dominant failure mode during the impact loading.

5.2. Verification using the experimental results reported by Greenhalgh *et al.* [54]

Greenhalgh *et al.* [54] investigated the influence of the material type, geometry of the structure such as the thickness of the skin and different spacing of the stringers, and position of the impact loading on stiffened laminated plates. They studied damage caused by impact using ultrasonic techniques and electron microscopy.

All stiffened carbon- fiber reinforced panels were made up of a skin and three I-section stringers which were co-cured in an autoclave. Panels geometries are shown in Figure 5.7. Three panels were manufactured from T800/524C carbon fiber reinforced that skin Stacking sequence of type 1 and type 2 were $[-45/0/+45/90]_{3s}$ and stacking sequence of type 3 was $[-45/0/+45/90]_{3s}$. The stringer parts were made of four laminates; a tapered foot, a cap and two C-Section laminates in between. The lay-up of the cap was while both C-Sections and the foot stacking sequence was . Mechanical properties of the using material are given in Table 5.2.

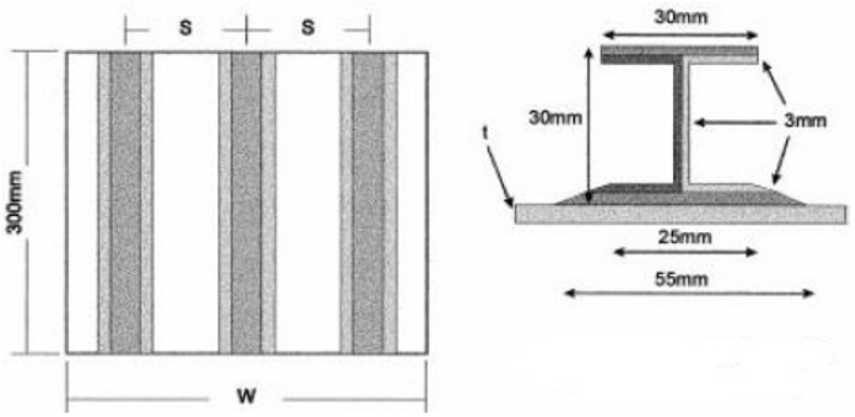

Figure 5.7. Geometries of the skin-stringer panel [11].

Table 5.2. Mechanical properties of T800/524 [54].

Parameters	**Values(GPa)**
E_1	160
E_2	9.2
G_{12}	6.2
X_t	1890
X_c	1615
Y_t	50
Y_c	250
S	105

5.2.1. Boundary conditions and low velocity impact details

All ended of the stiffened panels were placed in the epoxy resin and contained in an aluminum alloy section which were clamped to a horizontal steel plate. The low velocity impact was carried out by dropping an impactor to the stiffened plate. The impactor wit hemispherical nose with diameter of 10 mm was released from height of 1m to produce impact energy of 15 J. The impact locations in the tests were addressed in Figure 5.8.

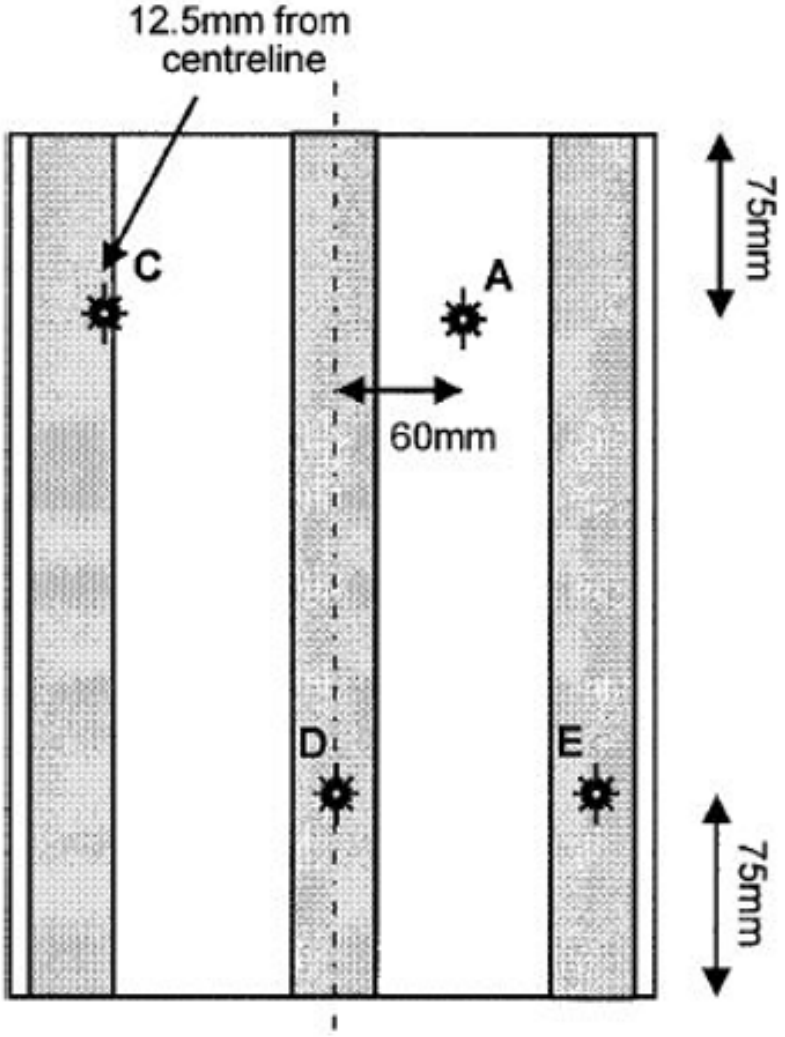

Figure 5.8. Impact locations [54].

5.2.2. Comparison of ANSYS/ LS-DYNA results with E.Greenhalgh's experimental results

In the current study, the stiffened plate is simulated by using ANSYS/LS-DYNA (Figure 5.9). All the impact and boundary conditions are the same with the reference. Tiebreak contacts are used to attach the stiffeners to the plate.

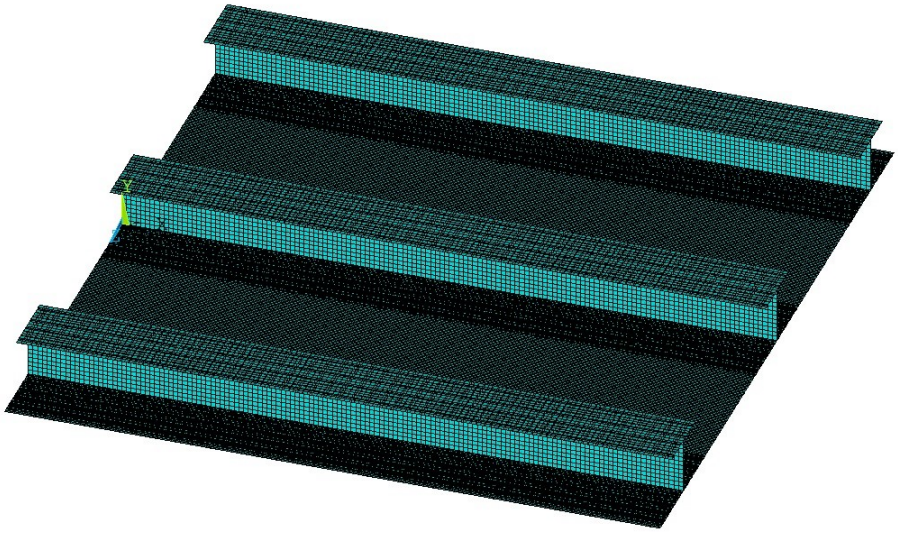

Figure 5.9. Simulated model of the stiffened plate.

In the experimental study, four cases were studied according to the impact location but the only case that is modeled in this study is the impact on the bay (point A in the Figure 5.8). In the reference, the obtained values for maximum contact force was 6157 N. in this study, its value is 5844. The percent error is 5 which indicates the perfect agreement between the results. The other parameter that was collected by Greenhalgh is the maximum deformation which is equal to 4.23 mm. Figure 5.9 shows the deformation plot at the load step in which the maximum deformation is happened in the simulated model. As it can be seen in figure 5.10, maximum deformation in the model is 4 mm which is close to the test result. By implementing Hashin delamination initiation criterion, it is observed that in several interfaces, the value of the criterion exceeds its limit and delamination happens as it was observed in the experimental results.

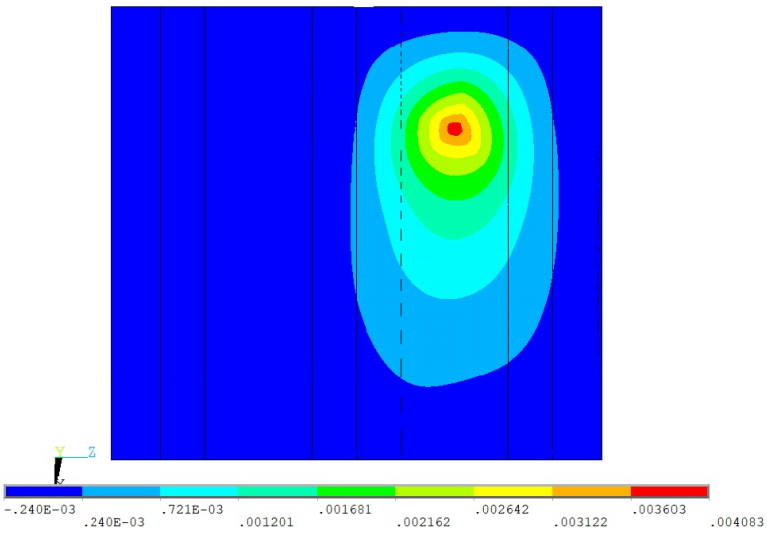

Figure 5.10. Deformation plot of the simulate model of the stiffened plate.

5.3. Mesh convergence analysis

In the finite element analysis, choosing the proper mesh size is very important. Because accuracy of a finite element model depends on it. Very coarse mesh size may give unrealistic results, finer mesh size also may result in unacceptable outcome and unnecessarily increase computational cost. Mesh- convergence analysis is performed for the stiffened plate subjected to static loading and impact loading. Figure 5.11 and Figure 5.12 show maximum deflection and equivalent stress of the stiffened plate respectively in the static load in different mesh sizes. Figure 5.13 and Figure 5.14 demonstrate deflection and equivalent stress graphs respectively in the impact load in different mesh sizes. These result are for a node which has maximum displacement during the loading. According to the figures the best element sizes are 8 mm×8 mm and 4 mm×4 mm for the static and impact loading respectively. In impact loading, it is notable that deflection converges at larger mesh sizes but Tsai-wu, and equivalent stress converge at 4 mm ×4 mm element size in which, by decreasing the mesh size from 4 mm ×4 mm, the results are approximately the same but solution time increases significantly.

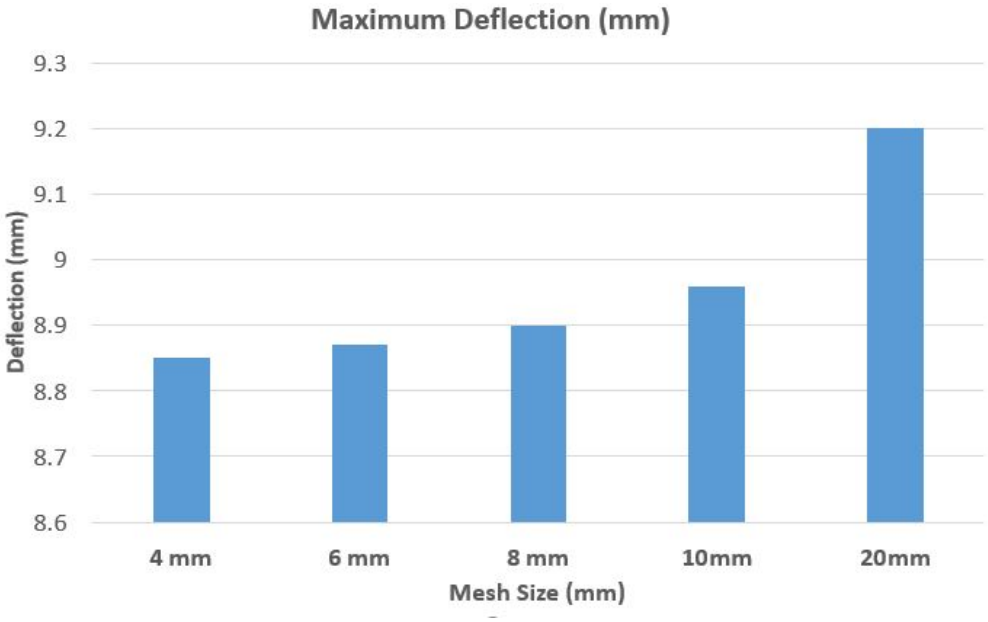

Figure 5.11. The convergence result for maximum deflection in static loading.

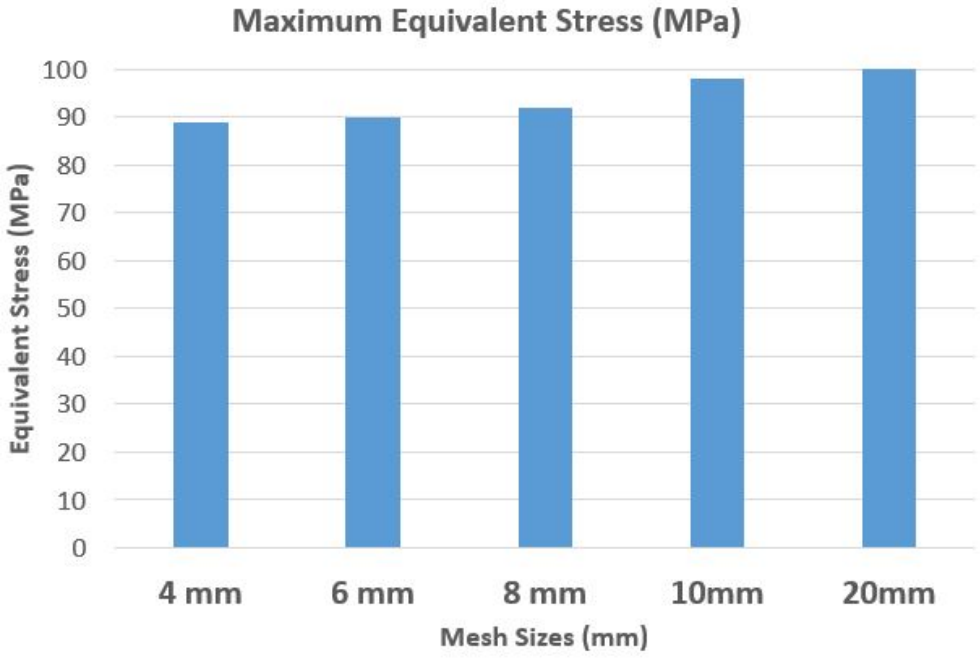

Figure 5.12. The convergence result for equivalent stress in static loading.

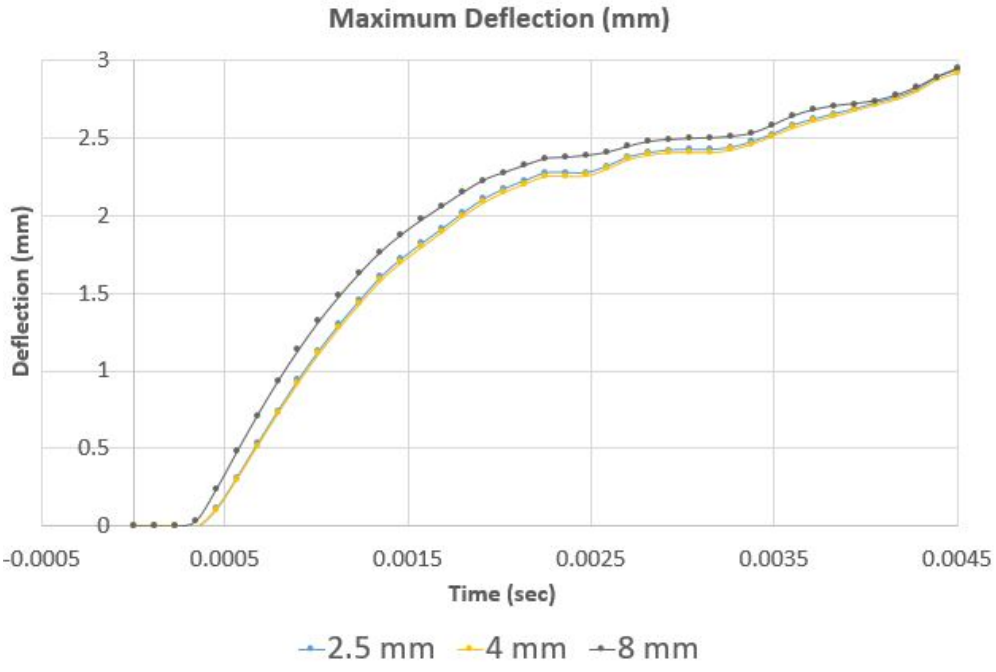

Figure 5.13. The convergence result for deflection in impact loading.

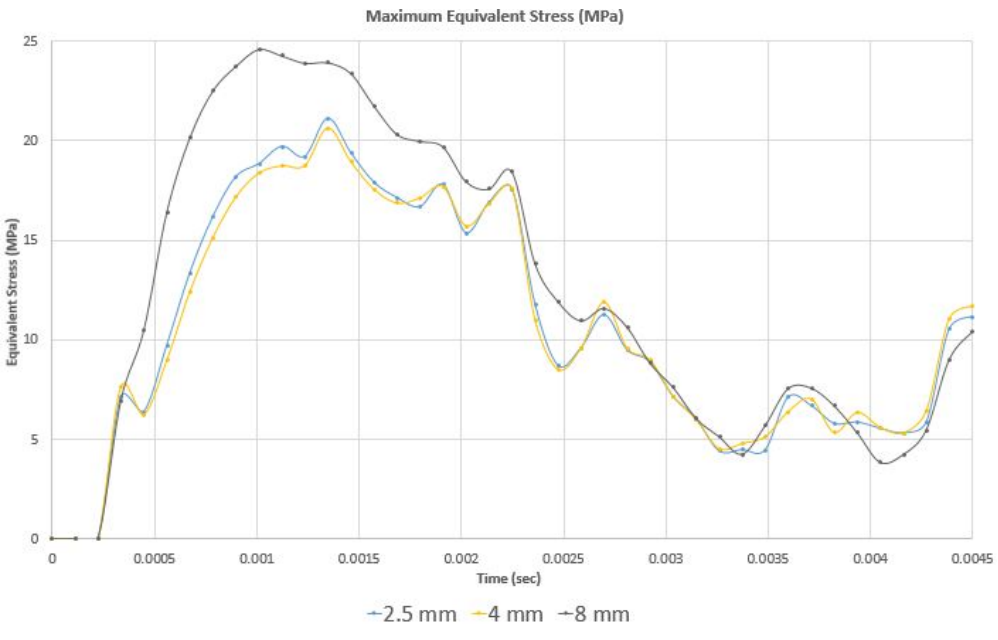

Figure 5.14. The convergence result for equivalent stress in impact loading.

6. RESULTS AND DISCUSSIONS

The optimum design for a hat-stiffened composite plate is obtained by coupling the modified simulated annealing algorithm with commercial finite element software ANSYS. The material used for this study is E-glass-fiber-reinforced composite. Its mechanical properties are given in Table 6.1.

Table 6.1. Mechanical properties and strengths of the E-glass fiber composite material [52].

Parameters	**Values**
E_1 (GPa)	53.48
E_2 (GPa)	17.7
G_{12} (GPa)	5.83
ν_{12} $(-)$	0.278
X_t (MPa)	1140
X_c (MPa)	570
Y_t (MPa)	35
Y_c (MPa)	114
SC (MPa)	72

The plate contains 20 plies; the thickness of each ply is 0.125 mm with a total thickness of 2.5 mm. Different numbers of plies are also tried. The stiffener contains 14 layers and its total thickness is 1.75 mm. The stacking sequence is chosen as: $[+45_2, -45_2, +45, -45, (90, 0)_2]_s$ for the plate and $[+45_2, -45_2, 90_2, 0]_s$ for the stiffener. Ply orientations are not varied in the optimization. The geometry of the plate is kept constant during the optimization process and its length is 0.8 m and its width is 1.0 m.

The major goal for the optimization is to increase impact resistance with minimum use of material. In this study, the optimization process is performed on the stiffened plate for a static loading case and three impact loading cases (Table 6.2). In the static loading, the stiffened plate is subjected to a transverse force with a magnitude of 700 N and this force is distributed to an area with dimensions of 28 mm×28 mm at the center of the plate. In case A and case B, impactor collides on the center of the plate. Case C is a multi-loading case, collisions occur on different locations near the plate ends at different times.

Table 6.2. Simulated low velocity impact models.

Case	**Impact location Center=(0,0)**	**Impact energy(J)**	**Impactor velocity Just before the impact(m/s)**	**Impactor diameter**
A	Center of the plate	0.5	3.1	42
B	Center of the plate	0.48	3.0	54
C	(x,y)=(0,0.4) (x,y)=(0.3,0)	0.5	3.1	42

The optimum shapes of the stiffened plate obtained for the static loading case and impact loading cases A, B, and C are shown in Figures 6.1, 6.2, 6.3, and 6.4, respectively and their cross sections are shown in Figure 6.5.

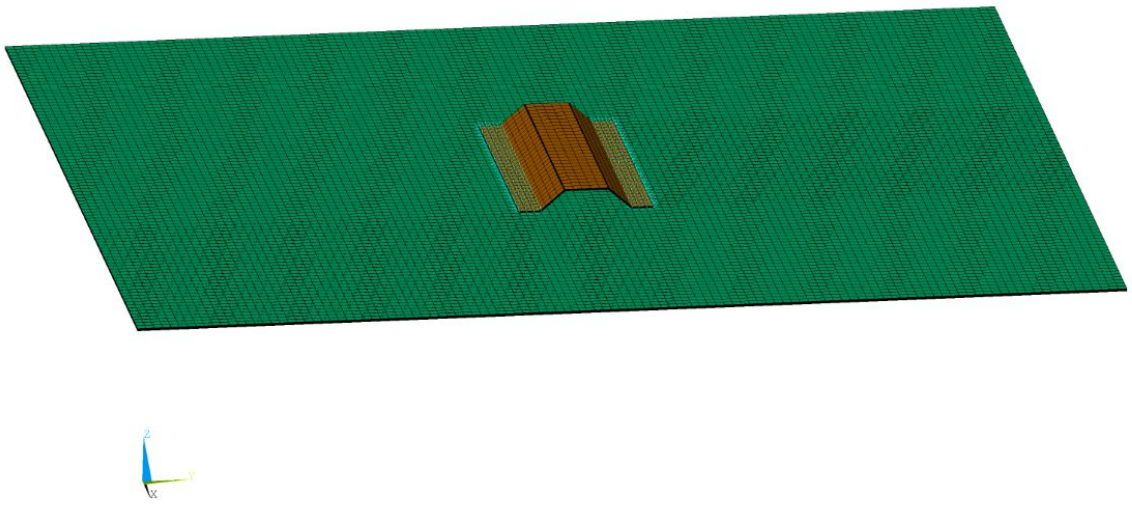

Figure 6.1. The stiffened plate optimized for the static loading.

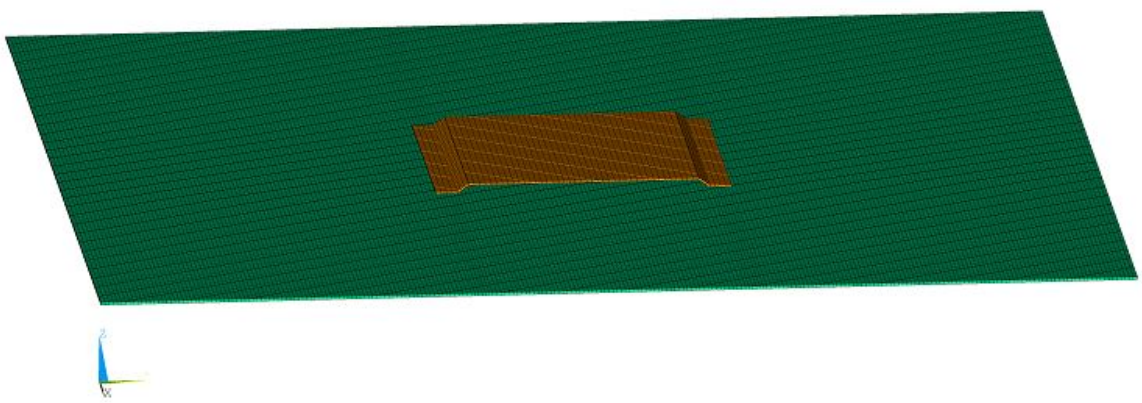

Figure 6.2. The stiffened plate optimized for loading case A (central impact).

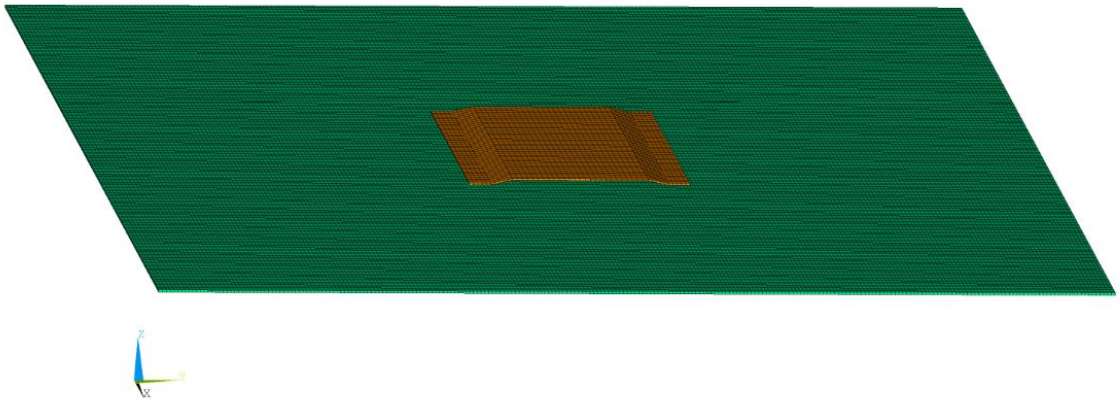

Figure 6.3. The stiffened plate optimized for loading case B.

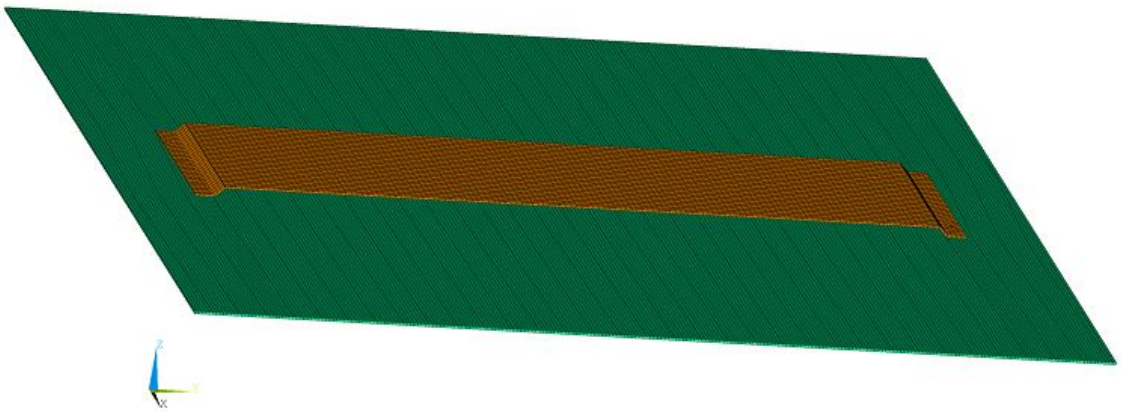

Figure 6.4. The stiffened plate optimized for loading case C (multi loading).

In impact-loading case C (multi-loading case), the impact that occurs near the longer edge of the plate (at location (0.3, 0) with the center location defined at (0,0)) is more critical compared to the impact closer to the shorter edge (at location (0, 0.4)) for the optimum shape. However, in some configurations generated during the optimization process, impact close to the shorter edge was more critical.

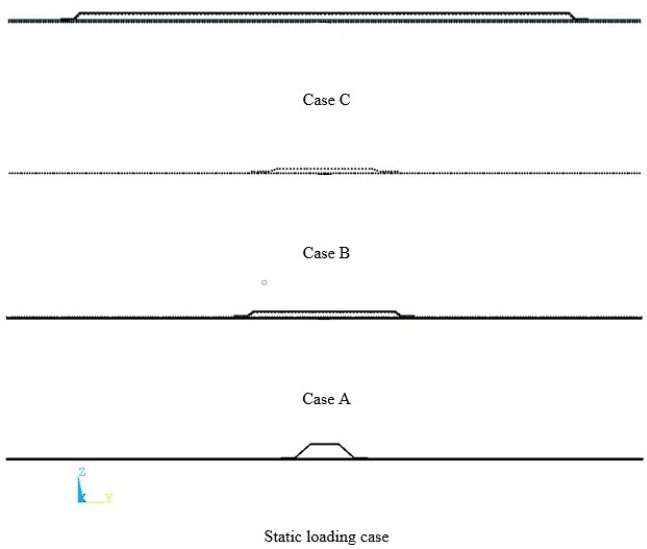

Figure 6.5. Cross sections of the optimum stiffened plates. Type C is optimized for multi-loading case, type B for central impact with larger impactor, type A for central impact, and the last one for transverse static force.

As it is seen in Table 6.3, width of the flange and height of the optimum stiffened plates are small in comparison to the length and width of the stiffener. This is because with a larger height of the cap and a larger width of the flange, the stiffness of the structure is increased which leads to a smaller deformation by the stiffened plate as a result of impact loading. Consequently, less amount of the impact energy can be absorbed by the stiffened plate and the structure is less likely to resist the failure. Table 6.4 gives the values of the weight, the maximum Tsai-Wu, and the maximum deflection of the stiffened and unstiffened plates under the static loading. Delamination results are not reported, because in none of the loading cases delamination failure of the plates is critical. The stiffened plate shows better performance than the plates without stiffener. The stiffener not only enhances the resistance to failure but also decreases the maximum deflection of the structure. As it can be seen in Table 6.4, the plate with thickness of 2.5 mm fails but when the plate is thicker it will tolerate failure; but the maximum deflection is still higher than the allowable value. By adding the stiffener optimized for static loading, failure is avoided and also the maximum

deflection is reduced to acceptable values without significant increase in weight.

Table 6.3. Geometries of the optimum stiffened plates.

Dimension values (mm)	**Static loading**	**Type A**	**Type B**	**Type C**
Length of the stiffener	241.97	200.26	212.80	191.17
Width of the stiffener	121.26	278.58	257.24	842.12
Width of the stiffener flange	22.11	20.22	30.03	20.096
Width of the stiffener cap	43.59	224.77	187.42	789.07
Height of the stiffener web	21.36	9.92	7.06	12.00

Table 6.4. The weight, the maximum Tsai-Wu, and the maximum deflection of some unstiffened plates and the optimized stiffened plates. The loading is transverse static force.

	Weight (N)	**Maximum deflection (mm)**	**Tsai-Wu (-)**
Plate (thickness=2.5 mm)	31.392	10.51	1.045
Plate (thickness=2.5 mm)	33.903	10.058	0.982
Optimum Stiffened plate	32.404	8.95	0.863

Table 6.5 demonstrates the results for impact loading case B, which is central impact of an impactor having the same energy, but a radius 8 mm larger than the other impactors. The plate with thickness of 2.5 mm fails under the loading. By increasing its thickness to 5 mm, its stiffness is increased and the plate resists the impact load; but, the weight of the plate is increased by two times the former one.

By adding the optimum stiffener to a 2.5 mm-thick plate, the impact resistance is sufficiently improved with a small increase in weight.

Table 6.5. The weight, the maximum Tsai-Wu, and the maximum deflection for some unstiffened plates under load case B and the stiffened plate optimized for loading case B, which is central impact with a larger impactor.

	Weight (N)	**Maximum deflection (mm)**	**Tsai-Wu (-)**
Plate (thickness=1.5 mm)	18.835	4.23	2.074
Plate (thickness=2.5 mm)	31.392	2.55	1.291
Plate (thickness=4.25 mm)	53.336	1.116	1.086
Plate (thickness=5 mm)	62.784	0.856	0.995
Optimum Stiffened plate	32.679	2.48	0.989

Table 6.6 and Table 6.7 give the maximum Tsai-Wu value, the maximum deflection and the weight of unstiffened plates with different thicknesses and the optimum stiffened plates under central impact loading case A and multi-loading case C, respectively. As seen in the results, none the unstiffened plates have sufficient impact resistance regardless of thickness. It shows that increasing the thickness of a composite plate is not an effective way of increasing the failure resistance in low-velocity impact. However, by adding a stiffener to the plate, the impact responses improve significantly. According to Table 6.6, the stiffened plate optimized for central impact (type A) tolerates the central impact without failure. On the other hand, the stiffened plate optimized for multi-loading case (type C) does not survive the central collision, but its impact response is much better than the unstiffened plates. According to Table

6.7, when collisions occur close to the edges, type A plate exhibits the worst performance. On the other hand, type C plate shows much better performance compared to the other cases. As for deflections, if the stiffener is optimized for impact loading, there is no improvement in the stiffness of the plate, the deflections of the stiffened plates are about the same as that of the base plate.

Table 6.6. The weight, the maximum Tsai-Wu, and the maximum deflection of some unstiffened plates and the optimized stiffened plates. The loading is case A, central impact.

	Weight (N)	**Maximum deflection (mm)**	**Tsai-Wu (-)**
Plate (thickness=1.5 mm)	18.835	4.24	2.154
Plate (thickness=2.5 mm)	31.392	2.56	1.345
Plate (thickness=4.25 mm)	53.366	1.17	1.14
Plate (thickness=5 mm)	62.784	0.787	1.078
Optimum stiffened -plate type A	32.987	2.54	0.997
Optimum stiffened -plate type B	38.843	2.58	1.057

Table 6.7. The weight, the maximum Tsai-Wu, and the maximum deflection of some unstiffened plates and the optimized stiffened plates. The loading is case C, which is the multi- loading case.

	Weight (N)	**Maximum deflection (mm)**	**Tsai-Wu (-)**
Plate (thickness=1.5 mm)	18.835	4.06	2.435
Plate (thickness=2.5 mm)	31.392	2.31	1.373
Plate (thickness=4.25 mm)	53.366	0.0959	1.109
Plate (thickness=5 mm)	62.784	0.721	1.08
Optimum stiffened -plate type A	32.987	2.30	3.8
Optimum stiffened -plate type B	38.843	2.29	1.034

In summary, it is observed that the stiffened plate type C has the best performance in the impact loadings. The weight of its stiffener is about 25% of its base plate; then there is no significant increase in weight. It can survive collisions occurring at different locations with an impact energy reduced about 5-10 percent. Figure 6.6 and Figure 6.7 show displacement and equivalent contour plots respectively for first ply of the plate for stiffened plate type C subjected to impact loading case C. In Figure 6.8 and Figure 6.9 displacement and equivalent contour plots for first ply of the plate are shown respectively for stiffened plate type C subjected to central impact case A.

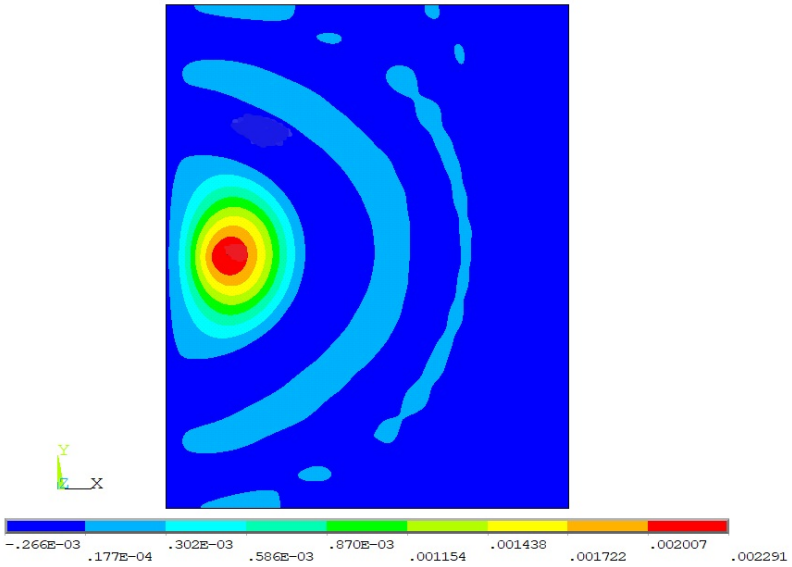

Figure 6.6. Displacement contour plot of stiffened plate type C in impact case C.

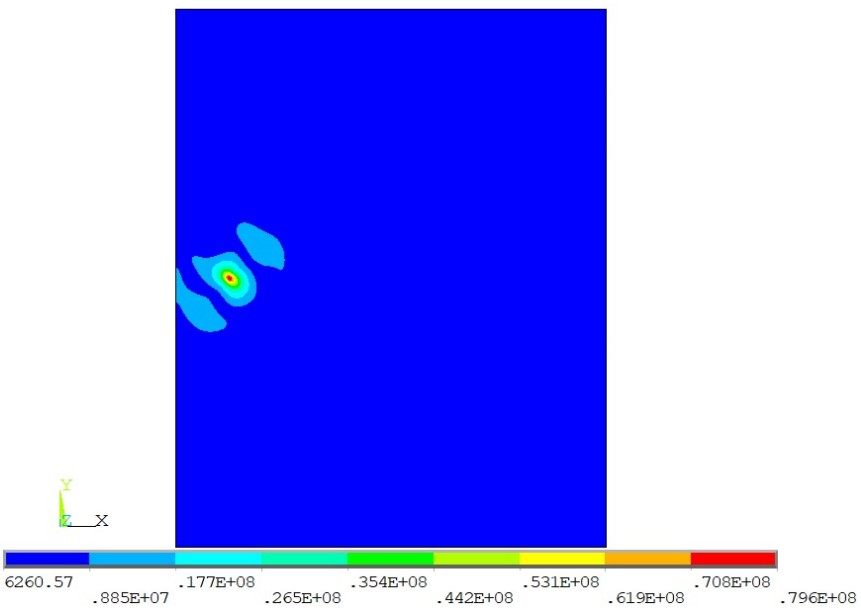

Figure 6.7. Contour plot of equivalent stress of stiffened plate type C in impact case C.

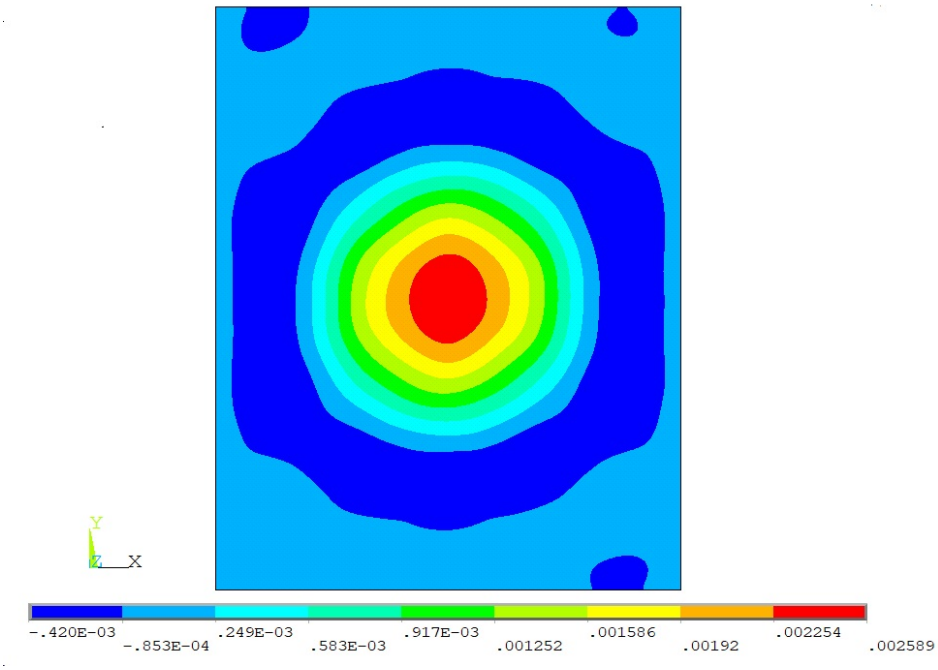

Figure 6.8. Displacement contour plot of stiffened plate type C in impact case A.

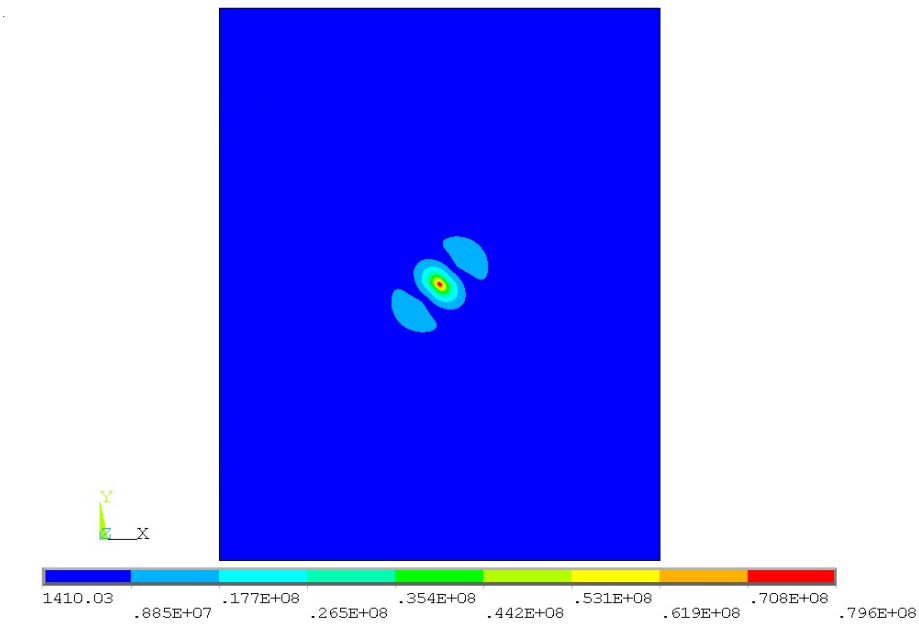

Figure 6.9. Contour plot of equivalent stress of stiffened plate type C in impact case A.

7. FUTURE WORKS AND RECOMMENDATIONS

In this study, the failure resistance of a composite plate subjected to a low velocity impact and transverse static force is improved by attaching an optimally design stiffener to it. The optimization variables are length of the stiffener, width of the flange, width of the cap and height of the stiffener. For further improvements in impact response of a stiffened plate, variables for optimum design can be taken as thickness, stacking sequence and ply orientation of the plate and the stiffener. In addition, using more than one stiffener and optimizing their distance from each other may influence impact response of the stiffened plate. In addition, the optimization is performed for hat-type stiffener. It is beneficial to try to find the optimum design of other stiffener types such as T-type, I-type and blade stiffeners. By comparing their impact performances, the best stiffener type can be determined.

8. CONCLUSION

The objective of the optimization in this study is to improve the impact resistance of plates with minimum use of material. A finite element model is developed to simulate the behavior of stiffened composite plates subjected to a transverse static and low-velocity impact loadings. A modified simulated annealing algorithm is utilized to find the optimum design. A hat-type stiffener is chosen and its geometrical parameters are taken as the design variables. To examine the intralaminar and interlaminar failure behavior in each iteration, Tsai-Wu and Hashin failure criteria are used, respectively. Stiffened plates are optimized for different loading conditions. Optimized stiffened plates and unstiffened plates of various thicknesses are compared as to their response in these loading conditions.

Unstiffened plates show low impact resistance; increasing the thickness does not significantly improve their impact performance. The impact resistance of the stiffened plates is much better than unstiffened ones. The stiffened plate optimized for central impact is better for central impacts, but worse for collision impacts on other locations. A stiffened plate is optimized for multi-loading cases in which two collisions occur near the edges at different times. This plate generally shows good impact performance for the impact loading cases considered in the present study.

Because the impact energy is low, in none of the loading cases, delamination failure is critical; the dominant failure mode is intralaminar failure.

If the stiffener is optimized for better impact performance, it does not considerably improve the stiffness of the plate. Deflections caused by impact loading on stiffened plates are about the same as that of the base plates.

REFERENCES

1. Jones, R., *Mechanics of Composite Materials*, Philadelphia, 2 edn., 1999.

2. Yap, J. W. H., M. L. Scott, R. S. Thomson and D. Hachenberg, "The analysis of skin-to-stiffener debonding in composite aerospace structures", *Composite Structures*, Vol. 57, pp. 425–435, 2002.

3. Goswami, S., "Failure analysis of polymer composite stiffened laminates using the finite element method", *Journal of Reinforced Plastics and Composites*, Vol. 18, pp. 2–14, 1999.

4. Prusty, B. G., "Progressive Failure Analysis of Laminated Unstiffened and Stiffened Composite Panels", *Journal of Reinforced Plastics and Composites*, Vol. 24, pp. 633–642, 2005.

5. Xie, M. and J. C. Chapman, "Design of web stiffeners: Axial forces", *Journal of Constructional Steel Research*, Vol. 59, pp. 1035–1056, 2003.

6. Gan, C., R. F. Gibson and G. M. Newaz, "Analytical/experimental investigation of energy absorption and grid-stiffened composite structures under transverse loading", *Experimental Mechanics*, Vol. 44, pp. 185–194, 2004.

7. Bedair, O., "Guidelines for Design of Transversely Stiffened Thin Walled Steel Plates", *Recent Patents on Engineering*, Vol. 10, pp. 69–76, 2016.

8. Frulla, G., P. Torino and I. Aeronautica, "Structural Behavior of Damaged Anisotropic Stiffened Panels Under Compressive Loads", *25th International Congress of the Aeronautical Sciences*, pp. 1–8.

9. Lee, K. C., J. Kang and C. H. Yoo, "Stiffness requirements for transverse stiffeners of rectangular CFT compression panels", *International Journal of Steel Structures*,

Vol. 13, pp. 265–274, 2013.

10. Found, M. S., I. C. Howard and A. P. Paran, "Impact behaviour of stiffened CFRP sections", *Composite Structures*, Vol. 39, pp. 229–235, 1997.

11. Greenhalgh, E., S. Singh, D. Hughes and D. Roberts, "Impact damage resistance and tolerance of stringer stiffened composite structures", *Plastics, Rubber and Composites*, Vol. 28, pp. 228–251, 1999.

12. Upadhyay, A. and V. Kalyanaraman, "Optimum design of fibre composite stiffened panels using genetic algorithms", *Engineering Optimization*, Vol. 33, pp. 201–220, 2000.

13. Stroud, W. J. and M. S. Anderson, "PASCO: Structural panel analysis and sizing code, capability and analytical foundations", *NASA TM-80181*, 1980.

14. Schmit, L. and B. Farshi, "Optimum design of laminated fibre composite plates", *International Journal for Numerical Methods in Engineering*, Vol. 11, pp. 623–640, 1977.

15. Nagendra, S., R. T. Haftka and Z. Gurdal, "PASCO-GA: A genetic algorithm based design procedure for stiffened composite panels under stability and strain constraints", *In Proceedings Tenth DOD/ NASA/FAA, Conf, on fiborous composites in structural design*, 1993.

16. Nagendra, S., D. Jestin, Z. Gürdal, R. T. Haftka and L. T. Watson, "Improved genetic algorithm for the design of stiffened composite panels", *Computers & Structures*, Vol. 58, pp. 543–555, 1996.

17. Bushnell, D. and W. D. Bushnell, "Optimum Design of Composite Stiffened Panels Under Combined Loading", *Computers & Structures*, Vol. 55, pp. 819–856, 1995.

18. Wang, X., J. S. Hansen and D. C. D. Oguamanam, "Layout Optimization of Stiffen-

ers in Stiffened Composite Plates with Thermal Residual Stresses", *Finite Elements in Analysis and Design*, Vol. 40, pp. 1233–1257, 2004.

19. Rikards, R., H. Abramovich and J. Auzins, "Surrogate models for optimum design of stiffened composite shells", *Computers & Structures*, Vol. 63, pp. 243–251, 2004.

20. Richardson, M. O. W. and M. J. Wisheart, "Review of low-velocity impact properties of composite materials", *Composites Part A: Applied Science and Manufacturing*, Vol. 27, pp. 1123–1131, 1996.

21. Sjoblom, P. O., J. T. Hartness and T. M. Cordell, "On Low-Velocity Impact Testing of Composite Materials", *Journal of Composite Materials*, Vol. 22, pp. 30–52, 1988.

22. Shivakumar, K. N., W. Elber and W. Illg, "Prediction of low-velocity impact damage in thin circular laminates", *AIAA Journal*, Vol. 23, pp. 442–449, 1985.

23. Strait, L. H., M. L. Karasek and M. F. Amateau, "Effects of Stacking Sequence on the Impact Resistance of Carbon Fiber Reinforced Thermoplastic Toughened Epoxy Laminates", *Journal of Composite Materials*, Vol. 26, pp. 1725–1740, 1992.

24. Aslan, Z., R. Karakuzu and B. Okutan, "The response of laminated composite plates under low-velocity impact loading", *Composite Structures*, Vol. 59, pp. 119–127, 2003.

25. Shyr, T. W. and Y. H. Pan, "Impact resistance and damage characteristics of composite laminates", *Composite Structures*, Vol. 62, pp. 193–203, 2003.

26. Belingardi, G. and R. Vadori, "Low velocity impact tests of laminate glass-fiber-epoxy matrix composite material plates", *International Journal of Impact Engineering*, Vol. 27, pp. 213–229, 2002.

27. Milani, A. S. and S. Yannacopoulos, "On Complexities of Impact Simulation of Fiber Reinforced Polymer Composites : A Simplified Modeling Framework", *The*

Scientific World Journal, Vol. 2014, 2014.

28. Naini, J. K. and P. R. Babu, "Impact Analysis of Embedded Delamination Location in Hybrid Curved Laminated Composite Stiffened Panel", *Applied Composite Materials*, Vol. 23, pp. 639–658, 2016.

29. Riccio, A., R. Ricchiuto, S. Saputo, A. Raimondo, F. Caputo, V. Antonucci and V. Lopresto, "Impact behaviour of omega stiffened composite panels", *Progress in Aerospace Sciences*, Vol. 81, pp. 41–48, 2016.

30. Chakraborty, R. D. and A. Dutta, "Optimization of FRP composites against impact induced failure using island model parallel genetic algorithm", *Composites Science and Technology*, Vol. 65, pp. 2003–2013, 2005.

31. Yong, M., B. G. Falzon and L. Ianucci, "On the application of genetic algorithms for optimising composites against impact loading", *International Journal of Impact Engineering*, Vol. 35, pp. 1293–1302, 2008.

32. Thompson, M. D., C. D. Eamon and M. Rais-Rohan, "Reliability-based optimization of fiber-reinforced polymer composite bridge deck panels", *Journal of Structural Engineering*, Vol. 132, pp. 1898–1906, 2006.

33. Jadhav, P. and P. R. Mantena, "Parametric optimization of grid-stiffened composite panels for maximizing their performance under transverse loading", *Composite Structures*, Vol. 77, pp. 353–363, 2007.

34. Gigliotti, M., A. Riccio, L. Iuspa, F. Scaramuzzino and L. Mormile, "Weight optimisation of damage resistant composite panels with a posteriori cost evaluation", *Composite Structures*, Vol. 88, pp. 312–322, 2009.

35. Carlsson, L. A., D. F. Adams and R. B. Pipes, "Basic experimental characterization of polymer matrix composite materials", *Polymer Reviews*, Vol. 53, pp. 277–302, 2013.

36. Song, K., C. Davila and C. Rose, "Guidelines and parameter selection for the simulation of progressive delamination", *ABAQUS User's Conference*, pp. 1–15, 2008.

37. Gigliotti, L., *Assessment of the applicability of XFEM in Abaqus for modeling crack growth in rubber*, Master Thesis, KTH School of Engineering Sciences, 2012.

38. Wisnom, M. R., "The role of delamination in failure of fibre-reinforced composites", *Philos Trans A Math Phys Eng Sci.*, Vol. 370, pp. 1850–1870, 2012.

39. Hashin, Z., "Failure Criteria for Unidirectional FibreComposites", *Journal of Applied Mechanics*, Vol. 47, pp. 329–334, 2018.

40. Norris, C. B., "Strength of orthotropic materials subjected to combined stresses", *Forest Products Laboratory*, pp. 1–41, 1962.

41. Chang, F. K. and K. Y. Chang, "A prograssive damage model for laminated composites containing stress concentrations", *Journal of Composite Materials*, Vol. 21, pp. 834–855, 1987.

42. Orifici, A. C., I. Herszberg and R. S. Thomson, "Review of methodologies for composite material modelling incorporating failure", *Composite Structures*, Vol. 86, pp. 194–210, 2008.

43. Kirkpatrick, S., C. D. Gelatt and M. P. Vecchi, "Optimization by Simulated Annealing", *Science*, Vol. 220, pp. 671–680, 1983.

44. Vakil-Baghmisheh, M. T. and A. Navarbaf, "A modified very fast simulated annealing algorithm", *2008 International Symposium on Telecommunications. IST 2008*, pp. 61–66, 2008.

45. Ali, M. M., A. To and S. Viitanen, "A direct search variant of the simulated annealing algorithm for optimization involving continuous variables", *Computers*

& Operations Research, Vol. 29, pp. 87–102, 2002.

46. Akbulut, M. and F. O. Sonmez, "Design optimization of laminated composites using a new variant of simulated annealing", *Computers and Structures*, Vol. 89, pp. 1712–1724, 2011.

47. Rodriguez, G., *Finite element modeling of delamination damage in carbon fiber laminates subjected to low-velocity impact and comparison with experimental impact tests*, Master Thesis, California Polytechnic State University, San Luis Obispo, 2016.

48. ANSYS, Inc., *Shell181*, 2018, `https://www.sharcnet.ca/Software/Ansys/16.2.3/en-us/help/ans_elem/Hlp_E_SHELL181.html`, accessed at December 2018.

49. Livermore Software Technology Corporation, *LS-DYNA Support*, 2010, `https://www.dynasupport.com/manuals/ls-dyna-manuals/LS-DYNA`, accessed at December 2018.

50. Erbil, E., *Impact loading in laminated composites*, Master Thesis, Dokuz Eylül University, 2008.

51. Rajbhandari, S. P., M. L. Scott, R. S. Thomson, D. Hachenberg, F. Bend and A. D. Gmbh, "An approach to modelling and predicting impact damage in composite structures", *ICAS Congress*, pp. 1–10, 2002.

52. de Macedo, R. Q., R. T. L. Ferreira, J. M. Guedes and M. V. Donadon, "Intraply failure criterion for unidirectional fiber reinforced composites by means of asymptotic homogenization", *Composite Structures*, Vol. 159, pp. 335–349, 2017.

53. Heimbs, S., S. Heller, P. Middendorf, F. Hähnel and J. Weiße, "Low velocity impact on CFRP plates with compressive preload: Test and modelling", *International Journal of Impact Engineering*, Vol. 36, pp. 1182–1193, 2009.

54. Greenhalgh, E., "Characterisation of impact damage in skin- stringer composite structures", *Composite Structures*, Vol. 36, pp. 187–207, 1997.